Seasonal Cycles and QBO Variations in Stratospheric CH_4 and H_2O Observed in *UARS* HALOE Data

WILLIAM J. RANDEL AND FEI WU

National Center for Atmospheric Research, Boulder, Colorado

JAMES M. RUSSELL III

Department of Physics, Hampton University, Hampton, Virginia

AIDAN ROCHE

Lockheed Martin Advanced Technology Center, Palo Alto, California

JOE W. WATERS

Jet Propulsion Laboratory, California Institute of Technology, Pasadena, California

(Manuscript received 9 December 1996, in final form 27 May 1997)

ABSTRACT

Measurements of stratospheric methane (CH_4) and water vapor (H_2O) are used to investigate seasonal and interannual variability in stratospheric transport. Data are from the Halogen Occultation Experiment (HALOE) on the *Upper Atmosphere Research Satellite* (*UARS*) spanning 1991–97. Profile measurements are binned according to analyzed potential vorticity fields (equivalent latitude mapping), and seasonal cycles are fit using harmonic regression analysis. Methane data from the *UARS* Cryogenic Limb Array Etalon Spectrometer and water vapor from the Microwave Limb Sounder are also used to fill in winter polar latitudes (where HALOE measurements are unavailable), yielding complete global seasonal cycles. These data reveal well-known seasonal variations with novel detail, including 1) the presence of enhanced latitudinal gradients (mixing barriers) in the subtropics and across the polar vortices, 2) strong descent inside the polar vortices during winter and spring, and 3) vigorous seasonality in the tropical upper stratosphere, related to seasonal upwelling and the semiannual oscillation. The observed variations are in agreement with aspects of the mean meridional circulation derived from stratospheric meteorological analyses. Interannual variations are also investigated, and a majority of the variance is found to be coherent with the equatorial quasibiennial oscillation (QBO). Strong QBO influence is found in the tropical upper stratosphere: the double-peaked ''rabbit ears'' structure occurs primarily during QBO westerlies. The QBO also modulates the latitudinal position of the tropical ''reservoir'' in the middle stratosphere.

1. Introduction

Important information on the transport and overall flow of mass in the stratosphere can be obtained by analysis of long-lived chemical constituents. Two such constituents are methane (CH_4) and water vapor (H_2O). Methane is produced by biotic activity near the earth's surface, is transported into the stratosphere in the Tropics, and chemically destroyed (oxidized) above 35 km. The photochemical lifetime of CH_4 below 40 km is $>$100 days, so the stratospheric distribution is determined mainly by the circulation. Methane measurements from satellites have been used in a number of studies to deduce stratospheric circulation features (e.g., Jones and Pyle 1984; Solomon et al. 1986; Gray and Pyle 1986; Holton and Choi 1988; Stanford et al. 1993; Russell et al. 1993a; Kumer et al. 1993; Bithell et al. 1994; Schoeberl et al. 1995). Likewise, water vapor has been used to deduce the global stratospheric circulation (Brewer 1949) and examine details of tropical (Mote et al. 1995, 1996) and global (Lahoz et al. 1996a; Rosenlof et al. 1997, hereafter RO97) transport. The ability to correctly simulate CH_4 and H_2O is a useful benchmark for numerical models of the middle atmosphere (e.g., Prather and Remsberg 1992).

The objective of this study is to analyze a long record (1991–97) of satellite CH_4 and H_2O measurements in order to quantify the seasonal cycle and interannual vari-

Corresponding author address: Dr. William J. Randel, Atmospheric Chemistry Division, National Center for Atmospheric Research, P.O. Box 3000, Boulder, CO 80307-3000.
E-mail: randel@ucar.edu

ability in stratospheric transport. The primary data are from the Halogen Occultation Experiment (HALOE) on the *Upper Atmosphere Research Satellite* (*UARS*). To fill in polar regions not sampled by HALOE, we use CH_4 measurements from the Cryogenic Limb Array Etalon Spectrometer (CLAES) and H_2O data from the Microwave Limb Sounder (MLS) instruments on *UARS* obtained during 1992–93. These combined data provide a complete global sample of the seasonal cycles of CH_4 and H_2O. Interannual variations are studied based on HALOE data alone.

The overall structure and variability of CH_4 is tightly coupled with H_2O in the stratosphere. This is because a principal source of stratospheric H_2O is from the oxidation of CH_4, via a series of chemical reactions that may be summarized (following Remsberg et al. 1984) by

$$CH_4 + 3O_2 + h\nu \rightarrow 2H_2O + CO + O_3.$$

This yields two molecules of H_2O for every one of CH_4. LeTexier et al. (1988) examined the chemistry in more detail and noted that some intermediate species may not be converted to H_2O, but that molecular hydrogen (H_2) could be produced. A conserved quantity in these chemical reactions is the total number of hydrogen atoms:

$$H_{total} = 2[H_2 + H_2O + \beta \times CH_4],$$

where β is a so-called chemical yield factor. Examination of data and model results have shown that H_2 is nearly constant and $\beta \sim 2.0$ over much of the stratosphere (Jones et al. 1986; Garcia and Solomon 1994; Dessler et al. 1994; Harries et al. 1996a; Remsberg et al. 1996). Thus the quantity $D = H_2O + 2 \times CH_4$ is an approximately conserved parameter. The result of this is that spatial gradients of CH_4 are approximate mirror images (with opposite sign) of those in H_2O, so that stratospheric transport variations are echoed in opposing signals in these two constituents.

There are two regions where H_2O data provide details of transport not seen in CH_4. First, a strong seasonal cycle is imparted to H_2O at the tropical tropopause from seasonal temperature variations, and this annual cycle is observed to propagate vertically in the tropical lower-middle stratosphere (Mote et al. 1995, 1996). Second, strong dehydration is observed in the Antarctic polar vortex during winter and spring (due to extreme cold temperatures), and this signal provides an opportunity to study transport across the edge of the vortex (Russell et al. 1993a; Tuck et al. 1993; Pierce et al. 1994; RO97). The seasonal cycle H_2O data presented here provide novel detail and global perspective to these features.

2. Data and analyses

a. HALOE data and equivalent latitude mapping

The primary data analyzed here are HALOE V18 vertical profile measurements of CH_4 and H_2O. The HALOE instrument is described in Russell et al. (1993b), and the CH_4 and H_2O data are discussed in detail in Park et al. (1996) and Harries et al. (1996b), respectively. We use HALOE level 3a data, which are available on 16 standard *UARS* pressure levels spanning 100–0.32 mb (approximately 16–56 km), with a vertical spacing of about 2.5 km. The time period analyzed here covers November 1991–March 1997.

HALOE is a solar occultation instrument that obtains 15 sunrise and 15 sunset measurements per day, each near the same latitude but spaced $\sim 24^\circ$ apart in longitude. The latitudinal sampling progresses in time, so that much of the latitude range 60°N–S is sampled in 1 month. One method to analyze the latitude–height structure of these data is to construct zonal means by simple longitudinal averaging. However, this has the disadvantage of averaging airmasses that may be physically distinct, in particular those inside versus outside the polar vortex [for cases when the vortex is elongated or not centered over the pole; see the example Plate 1 of Schoeberl et al. (1995)].

An alternative method is to average data along potential vorticity (PV) contours, which acts as an approximate vortex-following coordinate (McIntyre and Palmer 1983; Buchart and Remsberg 1986; Schoeberl et al. 1989, 1992, 1995; Norton 1994; Manney et al. 1995). For the analyses presented here we have derived PV from daily wind and temperature fields output from the United Kingdom Meteorological Office (UKMO) stratospheric data assimilation system (Swinbank and O'Neill 1994). The utility of PV versus zonal averaging is illustrated in Fig. 1, showing HALOE CH_4 measurements at 10 mb during September–October 1993 plotted versus latitude and versus PV. (Here and throughout the rest of this work the PV coordinate is expressed in terms of ''equivalent latitude,'' i.e., the latitude of an equivalent PV distribution arranged symmetrically about the pole.) The distribution of CH_4 versus latitude in Fig. 1 shows a wide scatter over high southern latitudes, due to sampling inside (low CH_4) and outside (high CH_4) of the polar vortex. Conversely, the CH_4 shows strong correlation with PV, with pronounced separation of vortex interior data (see also Bithell et al. 1994; Schoeberl et al. 1995). In a similar manner, HALOE H_2O data are found to be correlated with the polar vortex (Pierce et al. 1994; RO97) and associated PV fields.

Figure 2 shows an example of the PV mapping of HALOE CH_4 for data during January 1994. The PV mapping is done on each *UARS* pressure level separately (one can choose to perform the PV mapping using potential temperature as a vertical coordinate, but this involves vertical interpolations before and after mapping, and gives nearly identical results to mapping on pressure levels used here). Data are analyzed between 80°N and 80°S (as available for each month) on a 4° equivalent latitude grid. There are two advantages to the PV mapping: 1) data that are physically distinct remain separated; and 2) there is an increase in the effective latitude range of the data, as measurements inside the vortex

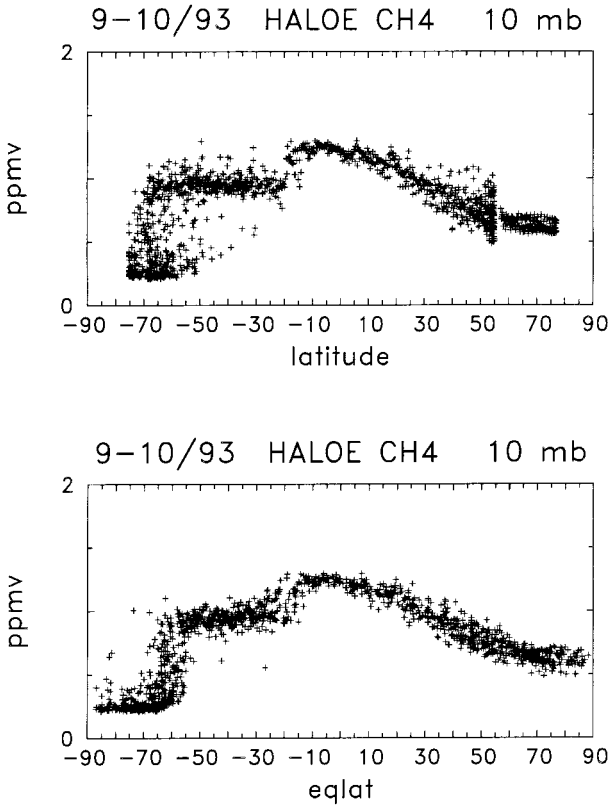

FIG. 1. Scatter diagrams of HALOE CH_4 observations at 10 mb during September–October 1993 plotted as a function of latitude (top) and potential vorticity (PV) (bottom). Potential vorticity is expressed in terms of equivalent latitude.

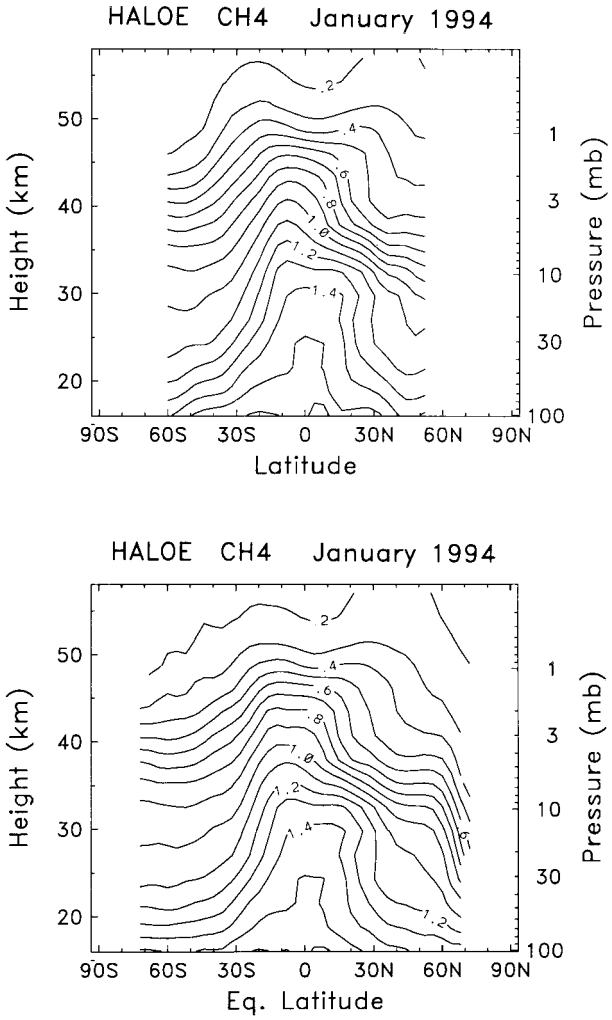

FIG. 2. Comparison of HALOE CH_4 observations during January 1994 calculated using zonal averages (top) and averages along PV contours (equivalent latitude mapping—bottom).

correspond to high equivalent latitude (note the NH data shown in Fig. 2). The equivalent latitude data (over 80°N–S) are binned into monthly samples prior to further analyses; we note these are not true monthly means, as data at different latitudes are observed at different times during each month. We require at least three data points at a particular altitude and equivalent latitude or else the corresponding monthly sample is left blank.

b. Seasonal cycle fits

Seasonal cycles are estimated from the monthly binned data by the fitting of seasonal harmonics at each (equivalent) latitude and pressure altitude. This method works well for the irregularly sampled HALOE measurements [similar analyses are used by McCormick et al. (1993)]. Examples are shown in Fig. 3 for CH_4 and H_2O data at 10 mb and 28°S. These show the monthly sampled equivalent latitude data (as ''plus'' signs), together with the harmonically varying seasonal cycles (the repeating smooth curves). The seasonal cycle at each location is determined using a time mean, plus annual and semiannual harmonics fit by least squares regression. The linear trend (determined over January 1993–December 1996) is removed prior to these seasonal fits, and it is also omitted from the interannual analyses discussed below. Note the opposing seasonality (and interannual variations) in the H_2O and CH_4 data in Fig. 3; this is a feature observed throughout the stratosphere in general, due to conservation of the quantity $D = H_2O + 2 \times CH_4$ (as discussed above).

Over high latitudes of both hemispheres, HALOE data are not available during several months in winter (the equivalent latitude PV mapping helps fill in this void in the NH, but less so during SH winter when the vortex is typically centered over the pole). For such high (equivalent) latitudes where data are unavailable each year, the seasonal cycle is only fit over months that data are available, and the remaining months are left blank [specifically, we require at least two years of data (out of five) for each individual month]. An example is shown in Fig. 4 for CH_4 data at 72°S, where no seasonal cycle is fit during April–August.

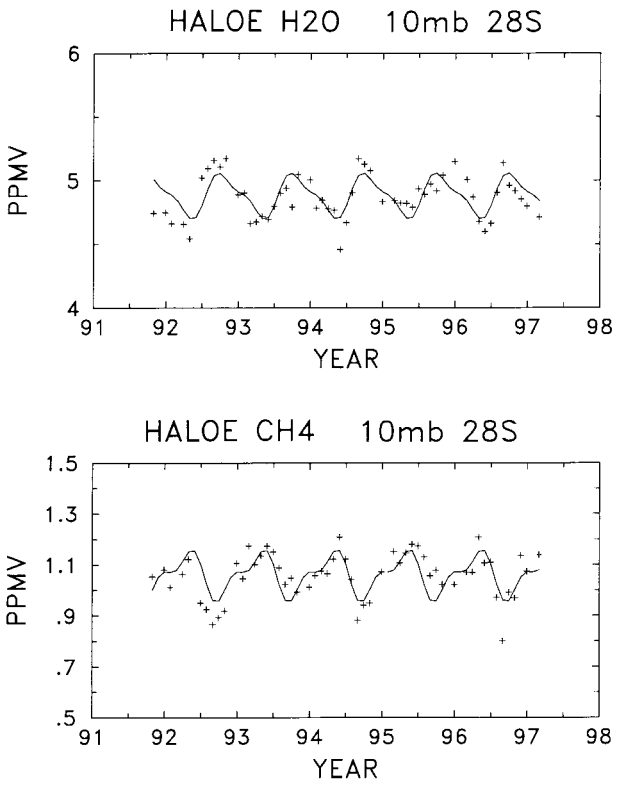

FIG. 3. Time series of HALOE H_2O and CH_4 data at 10 mb, 28°S. Crosses denote monthly mean data, and thin lines denote (repeating) seasonal cycles fit by harmonic regression.

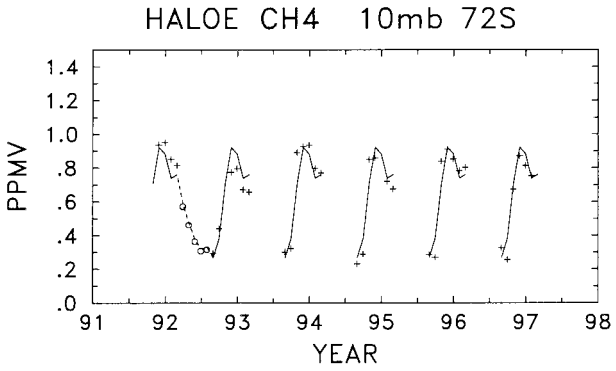

FIG. 4. Time series of CH_4 data at 10 mb, 72°S. Crosses and solid lines denote HALOE observations and fit seasonal cycle; note data are only available during September–February for each year. Circles and dashed lines during 1992–93 show adjusted CLAES data and seasonal cycle fit.

c. Addition of CLAES CH_4 and MLS H_2O data

In order to fill in the high latitude voids in the seasonal cycle estimates of CH_4, we include CH_4 observations from the CLAES instrument on *UARS* (Kumer et al. 1993; Roche et al. 1996). These data span a little more than one year (January 1992–April 1993), but offer more continuous sampling than the HALOE data, in particular observing the polar winter regions. The data used here are from the version 7 (V7) retrieval. The CLAES CH_4 data are mapped into equivalent latitude space and monthly averaged. Direct comparison of the CLAES and HALOE data shows reasonable agreement in the latitudinal structures, although there is an offset (bias), with CLAES approximately 20% higher than HALOE (as discussed in Roche et al. 1996). We remove this bias for the analyses here by simply adjusting the CLAES data (using a latitude-independent multiplicative factor) to match the HALOE measurements over a region adjacent to the missing HALOE data. This matching is done using a seasonal cycle fit of the CLAES data (over 1992–93) together with the seasonal cycle HALOE data (1991–97), in order to obtain smooth transitions. The adjusted CLAES data and fit seasonal cycle are included in the time series at 72°S shown in Fig. 4. Note the CLAES data are used only in the seasonal cycle estimates, since the short CLAES record precludes interannual analyses.

In a similar manner, we augment the HALOE seasonal cycle H_2O results using MLS data in polar regions. Stratospheric H_2O data are derived from MLS 183-GHz measurements, as described in Lahoz et al. (1996b). We use the version 4 (V4) retrieval for the analyses here, with time period spanning November 1991–April 1993. The seasonal cycle fit of the equivalent latitude MLS data are adjusted (by a small amount, ~5%) to smoothly match the HALOE seasonal cycle fit.

d. Calculation of residual mean circulation

Part of the results here include comparisons of the constituent seasonal cycles with estimates of the mean meridional circulation derived from United Kingdom Meteorological Office stratospheric analyses (Swinbank and O'Neill 1994). Specifically, we calculate monthly average components of the residual mean meridional circulation ($\overline{v}^*$, $\overline{w}^*$) using the coupled transformed Eulerian-mean (TEM) thermodynamic and continuity equations (as in Solomon et al. 1986; Rosenlof 1995). Radiative heating rates were calculated from an accurate radiative transfer code (Olaguer et al. 1992), incorporating UKMO temperatures, HALOE ozone, water vapor and methane, and climatological distributions of other trace gases. The overall circulation features are very similar to previous calculations (e.g., Gille et al. 1987; Eluszkiewcz et al. 1996). Aspects of constituent transport are studied based on the TEM constituent continuity equation [Andrews et al. 1987, their Eq. (9.4.13)]:

$$\frac{\partial \overline{\chi}}{\partial t} = -\overline{v}^* \overline{\chi}_y - \overline{w}^* \overline{\chi}_z + \nabla \cdot \mathbf{M} + \overline{S}. \qquad (1)$$

Here $\overline{\chi}$ is the zonal-mean constituent mixing ratio, $\overline{v}^*$ and $\overline{w}^*$ are components of the TEM residual mean cir-

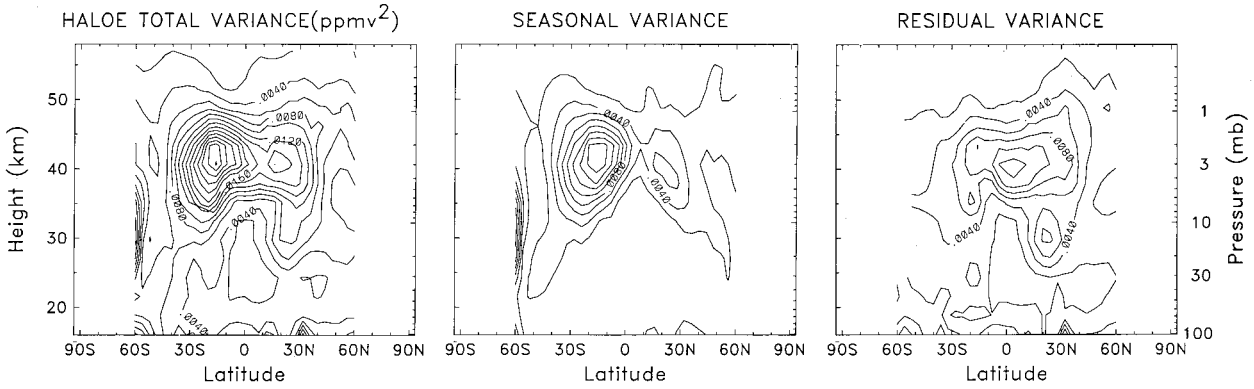

FIG. 5. Components of temporal variance in HALOE CH_4 data over 1991–97. Shown are total variance (left), seasonal cycle variance (middle), and residual interannual variance (right). Contours in all panels are 0.002 ppmv^2.

culation (discussed above), $\nabla \cdot \mathbf{M}$ is an eddy transport term, and $\overline{S}$ is a chemical source or sink term. This formalism has been used to study constituent transport in three-dimensional model simulations by Randel et al. (1994) and Strahan et al. (1996).

3. Seasonal variability

The overall temporal variance of the HALOE CH_4 data during 1991–97 is shown in Fig. 5, along with the component attributable to the harmonic seasonal cycle, and the residual (i.e., that attributable to interannual variance). Only HALOE data are used in these calculations, which span 60°N–S. Variance in all components peaks in the middle-upper stratosphere (over 30–50 km) over low latitudes. The overall variance is split fairly evenly between the seasonal and interannual components, but the spatial patterns are distinct (note the seasonal variance has a minimum over the equator, while the interannual variance has a maximum there). A majority of the interannual variance in Fig. 5 is associated with the QBO, as discussed below. Variance patterns in H_2O data (not shown) reveal upper stratospheric maxima similar to that in Fig. 5, with additional maxima in the Tropics over 20–30 km due to both seasonal and interannual components.

a. Global seasonality

Figure 6 shows the global structure of CH_4 in January, April, July, and October, derived from the seasonal cycle fits. The overall structures are similar to those shown previously (e.g., Luo et al. 1995; Park et al. 1996), but the synthesis of many years of data here allows the seasonality to be studied in some detail. Contours bulge upward in the Tropics and move latitudinally with season in the upper stratosphere, reflecting variations in the upward transport circulation in the Tropics (as shown below). There is a double-peaked pattern in the upper stratosphere in April related to the seasonal subtropical upwelling and the tropical semiannual oscillation (SAO); a similar double-peaked structure is not seen in October (the SAO is discussed in more detail below). Relatively strong horizontal gradients are seen in the subtropical lower stratosphere near 20°–30° N–S throughout much of the year, and strong gradients are also associated with the polar vortex in both hemispheres during winter–spring. These regions of enhanced gradients are associated with differential vertical advection (upward in the Tropics and downward in polar winter) and relative minima in horizontal mixing (so-called mixing barriers). The SH winter–spring polar vortex is particularly robust in these data, due to strong downward flow inside the vortex and small transport across the vortex edge (Russell et al. 1993a; Schoeberl et al. 1995; Fisher and O'Neill 1993; Manney et al. 1994; Sutton 1994). In contrast, the CH_4 contours are relatively flat over midlatitudes during winter–spring, showing evidence of more rapid mixing associated with the planetary waves (McIntyre and Palmer 1983, 1984; Leovy et al. 1985). There are relatively weak vertical gradients in high latitudes over 20–30 km during SH summer (January), possibly a remnant of very low (vortex) CH_4 following the SH final warming.

The corresponding seasonal cycle patterns in H_2O are shown in Fig. 7. The overall patterns are approximate mirror images of the CH_4 data in Fig. 6, including the seasonal movement of the upper-stratospheric maxima and appearance of a double peak in April. These similar patterns reflect the fact that the H_2O increase with altitude is due to CH_4 oxidation, so that total hydrogen is conserved (see references in introduction). This is demonstrated with the data here by calculation of the quantity $2CH_4 + H_2O$, shown for the October distribution in Fig. 8. Note the contour interval is identical between Figs. 7 and 8, so that the relative lack of spatial structure in $2CH_4 + H_2O$ (cf. H_2O or CH_4 alone) demonstrates that to first order $2CH_4 + H_2O \approx$ constant for these seasonal cycles. Two locations where this approximation does not hold

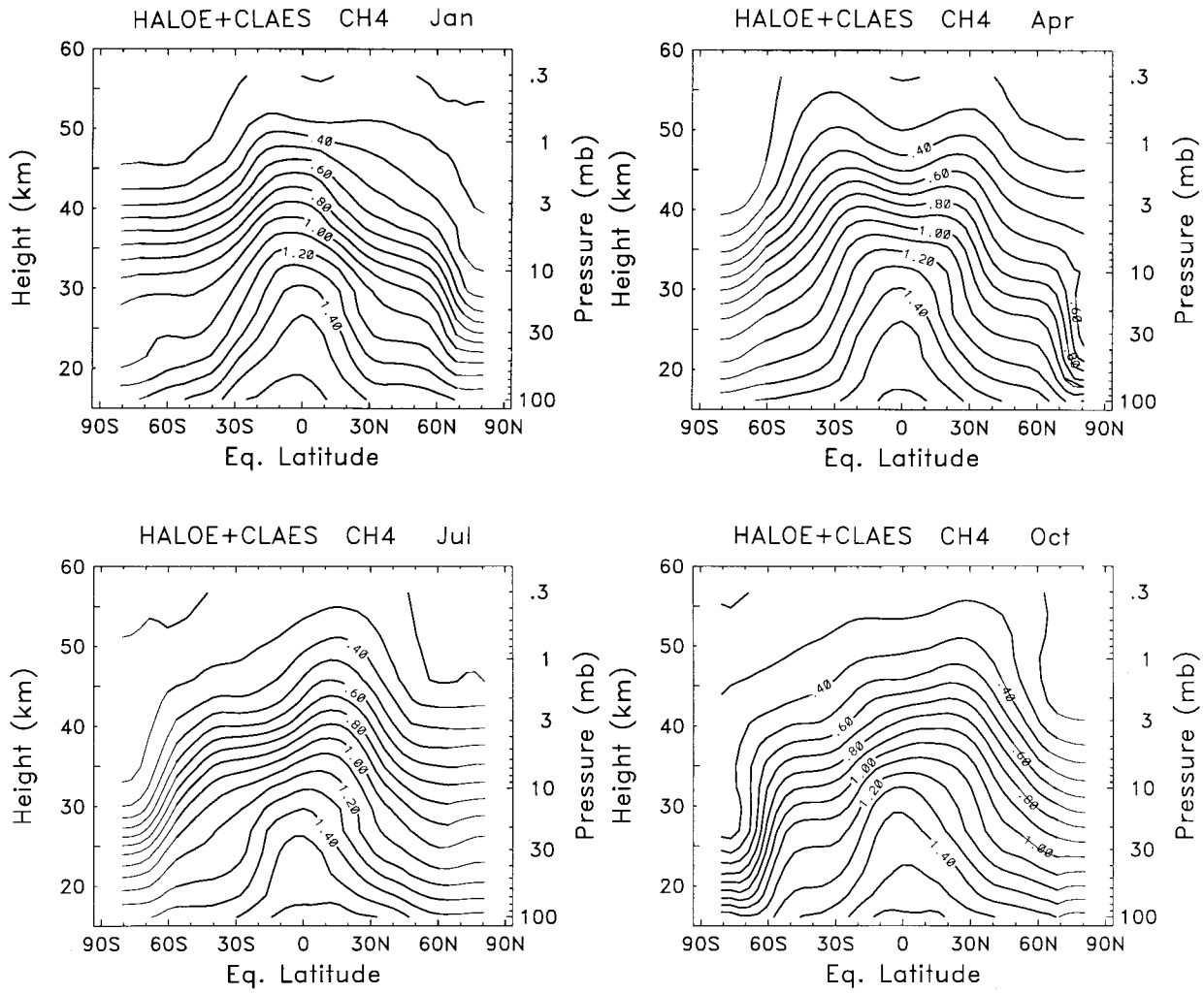

FIG. 6. Seasonal cycle estimates of CH_4 in January, April, July, and October. Contour interval is 0.1 ppmv.

are 1) in the tropical lower stratosphere, and 2) over Antarctica in winter–spring, as discussed in the introduction.

The latitude–time evolution of CH_4 at 68, 10, and 2.2 mb is shown in Fig. 9. There is a slight latitudinal shifting of the tropical maximum region in the lower stratosphere (68 mb) toward the respective summer hemisphere. Low CH_4 is observed in the springtime high latitudes of both hemispheres; these low polar values in the NH have received less attention than those in the SH (e.g., Russell et al. 1993a; Schoeberl et al. 1995), but appear very similar in these equivalent latitude data. These overall variations of CH_4 are in reasonable agreement with seasonality in the mean vertical circulation at 68 mb shown in Fig. 10 (calculated as discussed in section 2d). The patterns of high tropical CH_4 follow the upward velocity variations over low latitudes; note the weak tropical maximum during NH winter and the similar latitudinal movement of the contours (the $\overline{w}^* = 0$ contour is included in the lower panel in Fig. 9). Furthermore, there are springtime maxima in downward motion over both poles, in agreement with the corresponding minima in CH_4.

The CH_4 seasonal cycle in the middle stratosphere (10 mb) shows weakening of the midlatitude gradients during winter–spring in both hemispheres; this effect is more obvious in the SH. Similar midlatitude evolution at 10 mb is seen in the seasonal variation of nitrous oxide (N_2O) measured by CLAES (Randel et al. 1994). At 10 mb strong CH_4 gradients are seen across both polar vortices beginning in autumn, and the larger and stronger SH vortex is echoed in these CH_4 measurements.

Seasonality in the upper stratosphere (2.2 mb) is very different from the lower levels, showing a strong semiannual oscillation (SAO) with distinct maxima in the respective summer subtropics. These maxima are very similar to the patterns of vertical velocity at 2.2 mb (shown in Fig. 10), with the CH_4 maxima lagging the

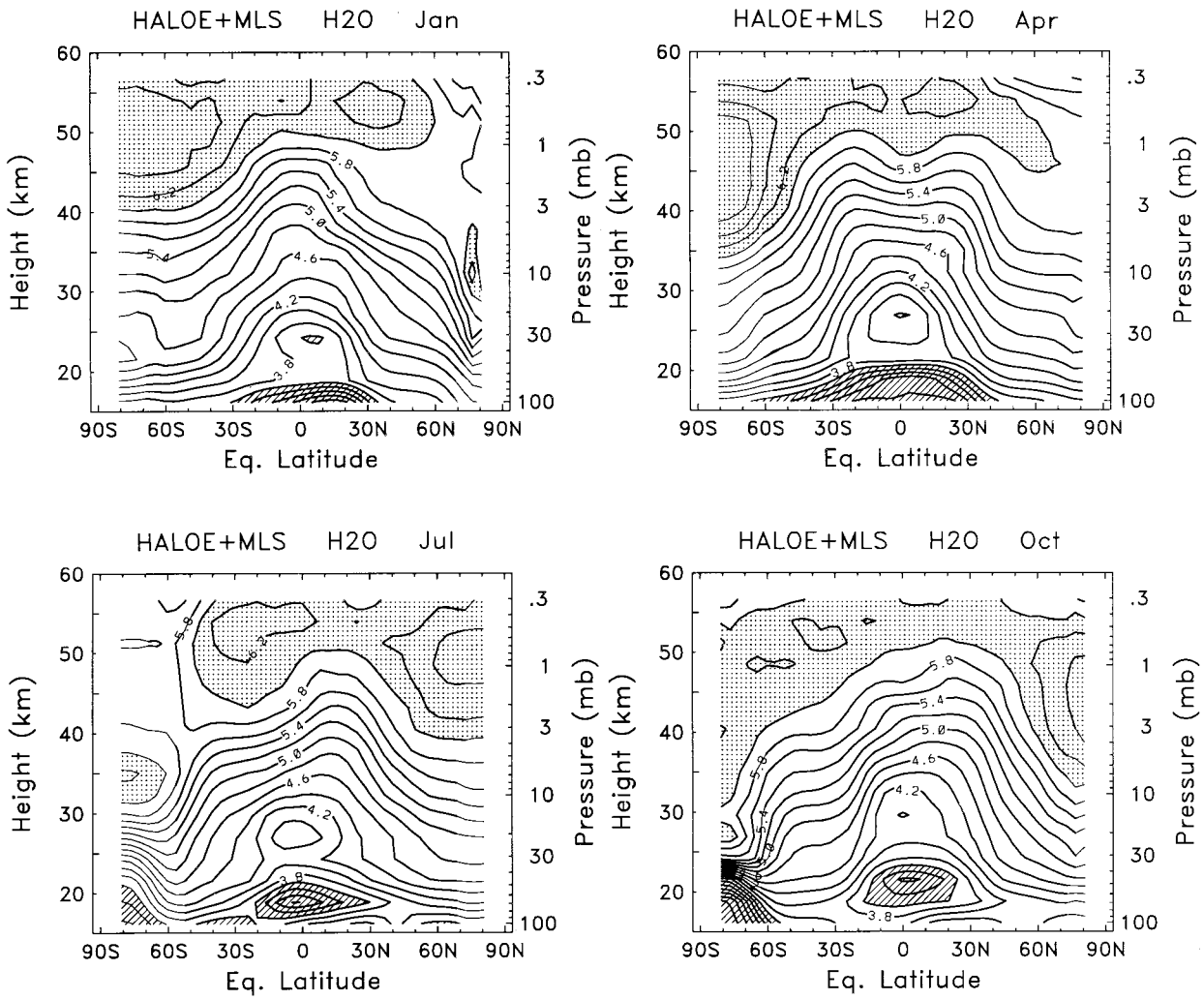

FIG. 7. Seasonal cycle estimates of H_2O in January, April, July, and October. Contour interval is 0.2 ppmv. Values below 3.6 ppmv are hatched, and values above 6.0 ppmv are stippled.

upward motion by approximately 1 month. A double-peaked latitudinal structure in CH_4 is seen over April–June.

Figure 11 shows the altitude–time variation of CH_4 at 76°N and S; note the time axes have been shifted in order to directly compare midwinter variations over both poles. The overall evolution is similar between hemispheres, with regular downward movement of the isolines during autumn and winter, followed by rapid elevation of the contours in spring (associated with breakup of the polar vortices and mixing in of midlatitude air). Somewhat lower CH_4 values are observed in the SH middle and upper stratosphere in winter, and the springtime transition is more dramatic and somewhat later in the SH; these aspects are due to the larger and more isolated SH polar vortex. The 0.3–0.8 isolines show consistent downward movement in the SH middle stratosphere during autumn and winter with a rate of -1.0 to -1.5 km month^{-1}; there is little downward movement in the lower stratosphere until spring (September–October), when values near -1.5 km month^{-1} (-0.6 mm s^{-1}) are inferred. These latter values are in excellent agreement with the downward velocities derived from the HALOE CH_4 data by Schoeberl et al. (1995), and with the TEM vertical velocities shown in Fig. 10 (see also Rosenfield et al. 1994). The NH middle stratosphere data (e.g., the 0.5 contour) yields descent rates near -1.5 km month^{-1}, similar to the SH. In the NH lower stratosphere the data in Fig. 11 shows a relative maximum in November–December (see also the lower panel of Fig. 9) that is inconsistent with the downward circulation in Fig. 10. This isolated feature is entirely due to the use of CLAES data during one year (1992), and its reality is suspect.

Figure 12 compares the observed wintertime variation of zonal-mean methane ($\overline{\chi}$) near the South Pole (76°S) with a transport calculation based solely on the mean vertical velocity $\overline{w^*}$:

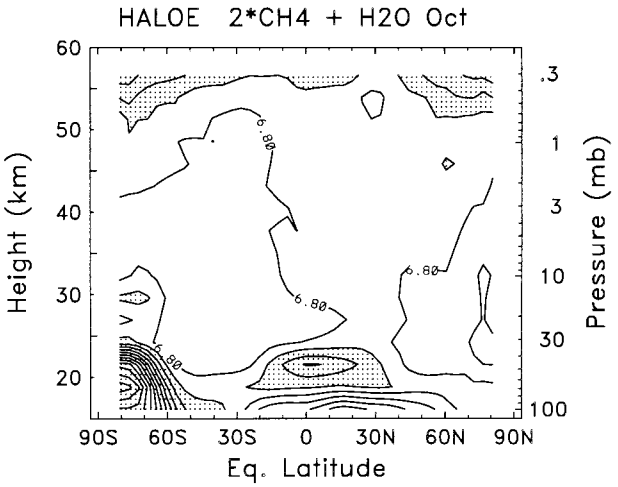

FIG. 8. Meridional cross section of the quantity $H_2O + 2CH_4$ in October, derived from the seasonal cycle H_2O and CH_4 data (Figs. 6 and 7). Contour interval is 0.2 ppmv, and values less than 6.6 ppmv are shaded.

$$\overline{\chi}(t) = \overline{\chi}(\text{March}) - \int_{\text{March}}^{t} \overline{w^*}\,\overline{\chi_z}\, dt. \qquad (2)$$

This is derived from Eq. (1), neglecting the $\overline{v^*}\,\overline{\chi_y}$, $\nabla\cdot\mathbf{M}$, and $\overline{S}$ terms. This is a reasonable approximation inside the Antarctic winter vortex, where $\overline{w^*}$ transport dominates $\overline{v^*}$, the chemical lifetime is very long ($\overline{S}$ is small), and eddy mixing with the vortex exterior is small (Bowman 1993; Chen et al. 1994; Strahan et al. 1996). March is chosen for the starting time as this is near the formation of the SH polar vortex, and the idea here is to test how well calculated descent rates in the vortex agree with observations (the comparisons go through October, just prior to vortex breakup). The comparisons in Fig. 12 show quite reasonable agreement at both the 10- and 46-mb levels. There is relatively strong downward motion in autumn (March–May) at 10 mb, followed by a relative minimum in $\overline{w^*}$ and more constant CH_4 in winter. At 46 mb there is relatively little downward motion until late winter–spring (see also Figs. 9 and 10). The approximate agreement in these comparisons provides a confirmation of the heating rates and vertical velocities derived from the meteorological analyses, and also supports the notion of vortex isolation in the SH (e.g., Bowman 1993; Chen et al. 1994; Manney et al. 1994; Bacmeister et al. 1995). Similar calculations in the NH (beginning in September) are shown in Fig. 13; here there is poor agreement, with the observed CH_4 changes much less than those calculated from $\overline{w^*}$. This is likely due to stronger meridional transport into and less isolation of the NH polar vortex.

Both NH and SH data in Fig. 11 show CH_4 minima (below 0.1 ppmv) near the stratopause during summer (see also the top panel in Fig. 9). These minima are due to rapid photochemical destruction of CH_4 over polar regions during summer (see Fig. 17 below); the cal-

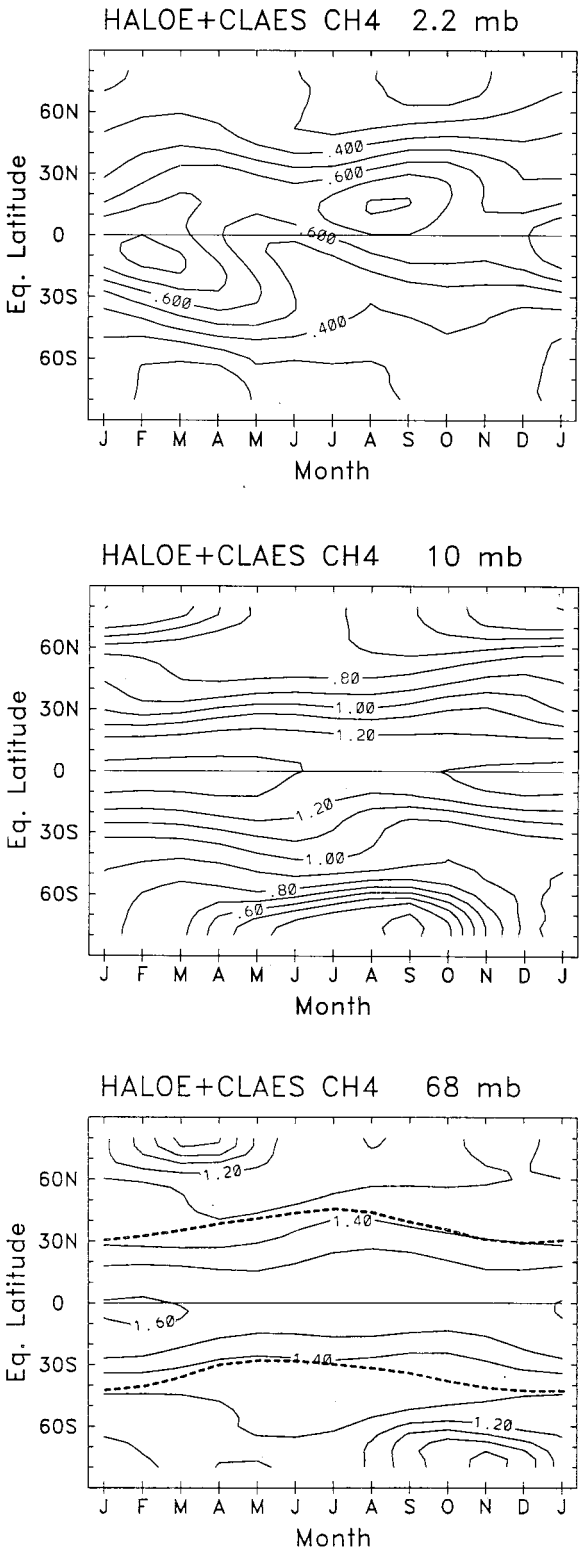

FIG. 9. Latitude–time sections of seasonal cycle variations in CH_4 at 2.2 mb (top), 10 mb (middle), and 68 mb (bottom). Contour interval is 0.01 ppmv. The dashed lines in the lower panel are the $\overline{w^*} = 0$ contours (from Fig. 10).

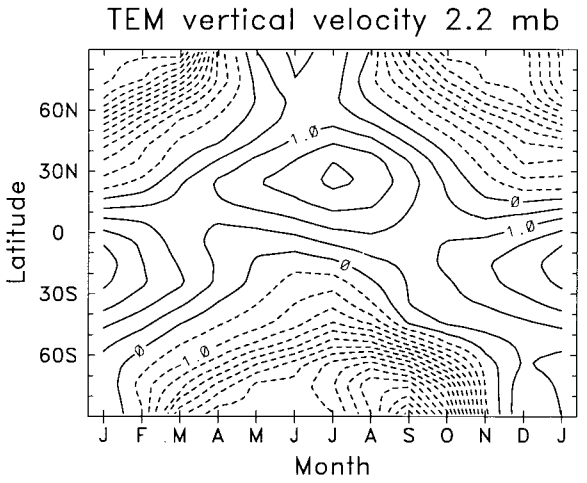

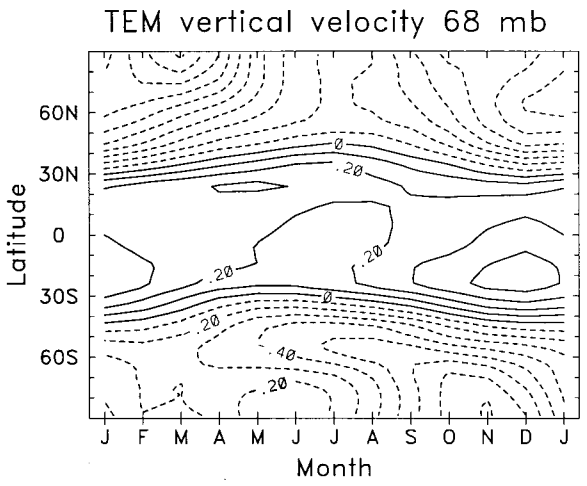

FIG. 10. Latitude–time sections of residual mean vertical velocity ($\overline{w^*}$) derived from UKMO data at 2.2 mb (top) and 68 mb (bottom). Contour intervals are 0.5 and 0.1 mm s^{-1}, respectively, and positive values denote upward motion.

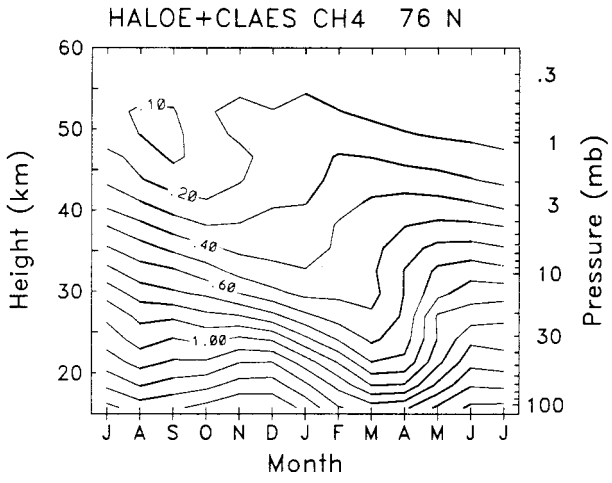

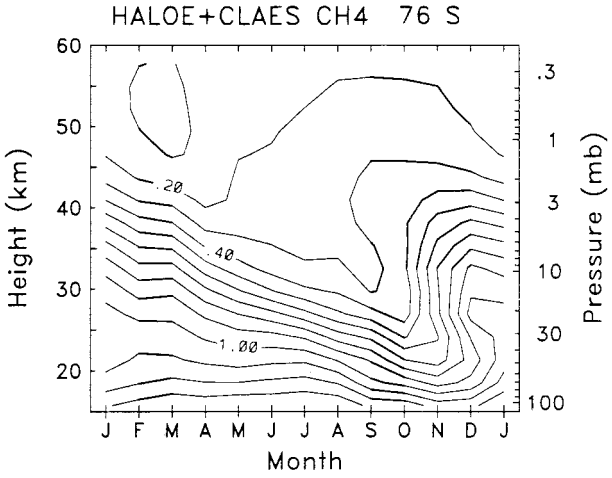

FIG. 11. Altitude–time sections of seasonal cycle variations in CH_4 at 76°N (top) and 76°S (bottom). Contour interval is 0.1 ppmv. Note the respective time axes are shifted by 6 months between the two panels.

culated photochemical lifetime of CH_4 in this region is near 1 month [see Fig. 1 of Solomon et al. (1986)].

b. Tropical variations

The altitude–time variations of both CH_4 and H_2O over the equator are shown in Fig. 14, which also includes diagrams with the respective time means removed at each altitude to highlight seasonality. There is a strong upward propagating annual variation in H_2O in the lower stratosphere, associated with the seasonal variation of tropical tropopause temperatures and the freezing out of H_2O in the tropical upwelling region [see extensive discussions in Mote et al. (1995) and (1996)]. A nearly identical pattern is seen in the total hydrogen $2CH_4 + H_2O$, as illustrated in a different manner in Fig. 15. Here the individual zonal means over 4° N–S are plotted, along with the associated harmonic fits, for pressure levels 100–10 mb (16–32 km). A strong annual cycle that progresses upward with time is observed over 100–32 mb; this cycle can be traced to 22 mb using the harmonic analysis, although there is substantially more interannual variability at this level. At 15 and 10 mb (29–32 km), the annual harmonic is relatively weak, and a semiannual component dominates at these levels (and above). The upward propagation of the annual signal over 100–32 mb (16–24 km) takes approximately 11 months; this corresponds to a vertical velocity of ~0.7 km $month^{-1}$ (~0.25 mm s^{-1}), in reasonable agreement with the tropical TEM vertical velocities in Fig. 10.

Figure 16 shows the space–time structure of both H_2O and $2CH_4 + H_2O$ at 100, 68, and 46 mb. While the annual cycles at 68 and 46 mb are approximately centered over the equator, variations at 100 mb are maxi-

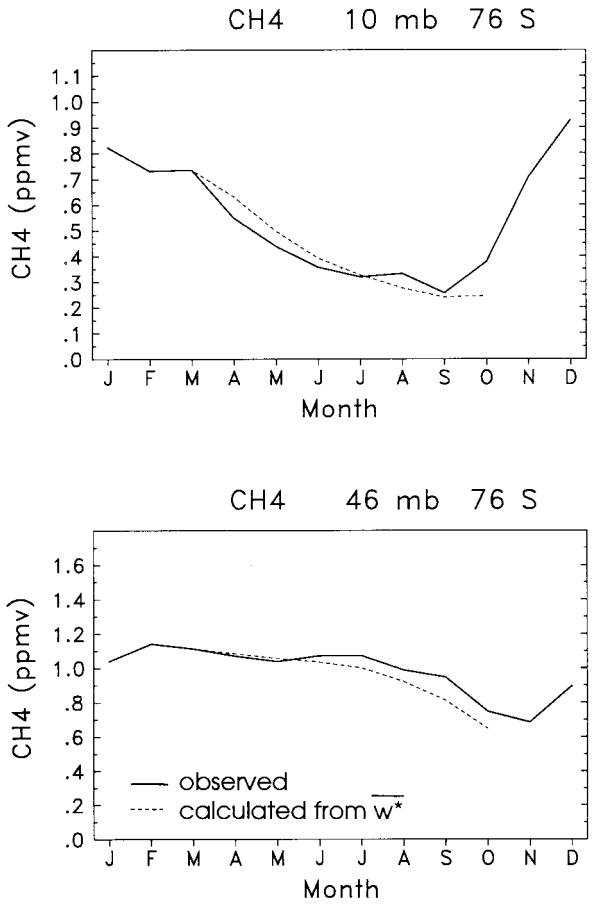

FIG. 12. Solid lines show seasonal cycles of CH_4 at 76°S, 10 mb (top), and 46 mb (bottom). Dashed lines show CH_4 estimated from $\overline{w^*}$ transport [Eq. (2)] between March and October.

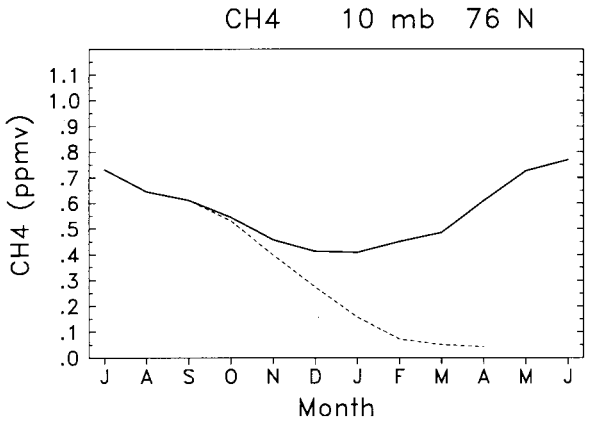

FIG. 13. Observed CH_4 variations at 76°N and 10 mb (solid line) and that calculated from $\overline{w^*}$ transport (dashed line).

mum near 15°–30°N. Lowest values are observed near 15°N in February–March, although the minimum 100-mb temperatures occur near the equator (e.g., Newell and Gould-Stewart 1981; Tuck et al. 1993). The maximum during NH summer (August–September) is even more asymmetrical, with maximum near 20°–30°N; this structure has little relation to zonal-mean temperatures. There is also a seasonal variation in meridional transport at 100 mb inferred in Fig. 16, with relatively little spreading of the low subtropical values into the NH during NH winter (note the strong gradients near 30°N), but stronger propagation of the NH summer maximum into high latitudes (with a time lag of order three months between 30° and 60°N). There is much less spreading of this maximum into SH midlatitudes. Based on analyses of these same HALOE H_2O data, RO97 discuss the asymmetry seen in Fig. 16 and note the meridional propagation of maximum values into NH midlatitudes. The asymmetry of these patterns (particularly the NH summer maximum) contribute to the higher values of H_2O observed in the NH versus SH lower stratosphere, as reported by Kelly et al. (1990). These data suggest the NH–SH asymmetry in the lower stratosphere is not due to asymmetric transport of equatorially centered maxima, but to dynamical processes in the NH subtropics (such as the Indian monsoon during NH summer). The enhanced meridional speading of the H_2O and $2CH_4 + H_2O$ at 100 mb compared to levels at and above 68 mb agrees with the results of Trepte et al. (1993), who present evidence for rapid meridional flow between Tropics and midlatitudes below 20 km, but not above this altitude. Similar results were inferred from the aerosol observations in Grant et al. (1994). This behavior is consistent with the tropical vertical velocity profile discussed by RO97: there is a minimum in $\overline{w^*}$ near 50–70 mb, such that only 20% of the upward mass flux at 100 mb continues upward across this level (with the remaining 80% moving laterally to either hemisphere). The data in Fig. 16 also provide convincing evidence that there is not strong mixing of the dehydrated SH polar vortex air into midlatitudes following vortex breakup (as also noted by RO97).

The H_2O data at 68 and 46 mb in Fig. 16 show minimum values in the Tropics and relatively strong horizontal gradients near both 30°N and 30°S, similar (but opposite) to the CH_4 latitudinal structure seen in Fig. 9. The lack of such gradients in the quantity $2CH_4 + H_2O$ (i.e., the 46-mb plot in Fig. 16) implies that it is the downward transport of photochemically aged air in the extratropics, plus a lack of rapid meridional mixing with the Tropics, that is responsible for these latitudinal H_2O gradients. Seasonal variations in both H_2O and $2CH_4 + H_2O$ show that the upward propagating tropical annual cycle is confined to ~30°N–S.

Inspection of Fig. 16 and the time series in Fig. 15 shows an attenuation of the amplitude of this annual cycle over 100–32 mb (in both H_2O and $2CH_4 + H_2O$) from approximately 1.5 to 0.7 ppmv; the attenuation is most rapid between 100 and 68 mb. Above 68 mb, where the tropical signal appears isolated from midlatitudes, the annual amplitude decreases from 1.1 to 0.7 ppmv between 68 and 32 mb. Supposing that this attenuation is due entirely to the mixing in of extratropical air (with

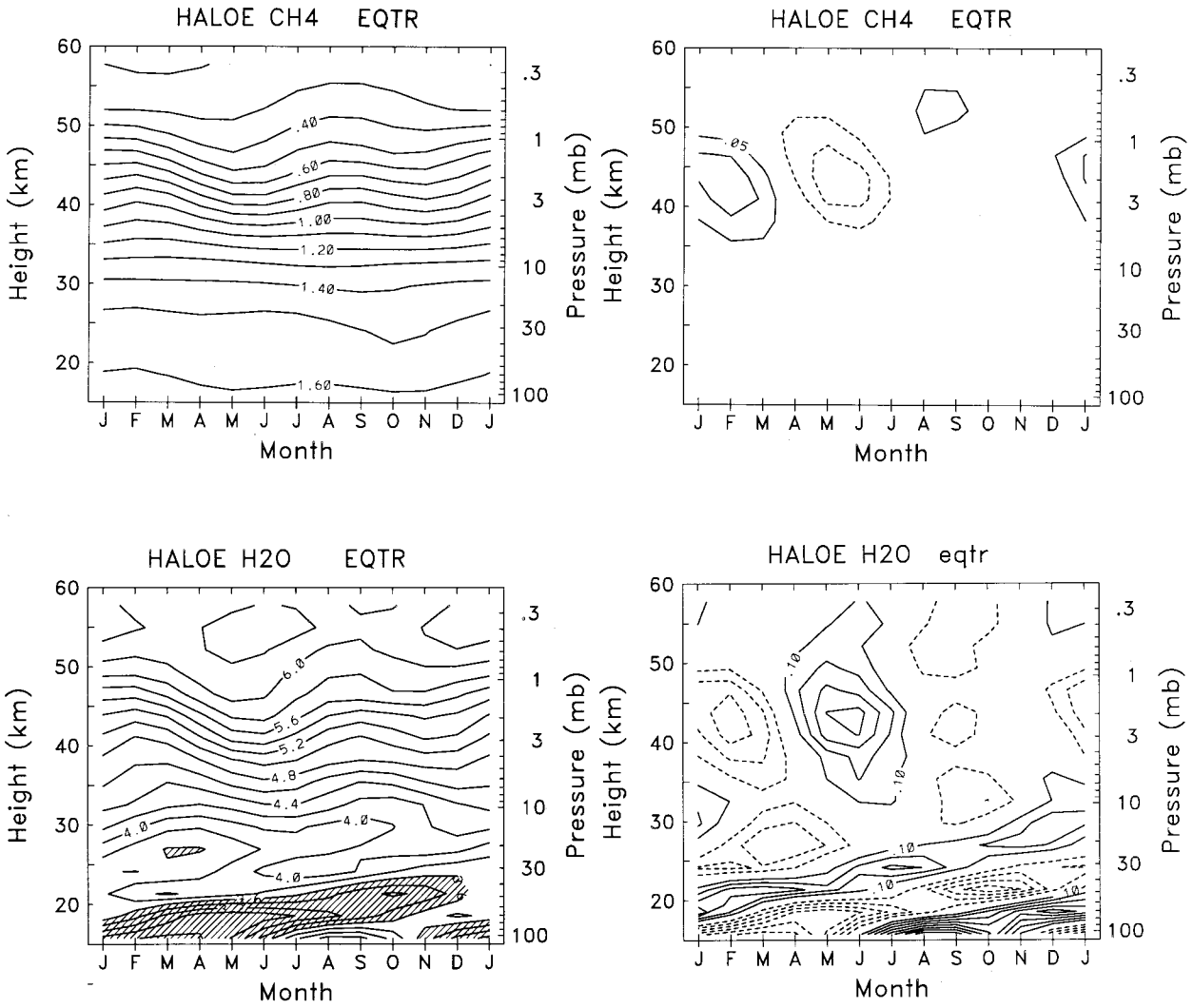

FIG. 14. Altitude–time sections of seasonal cycle variations in CH_4 (top) and H_2O (bottom) over the equator. Left panels show full fields, while right panels show seasonal anomalies (calculated by subtracting the time means at each pressure level). Values below 3.6 ppmv in the lower-left panel are shaded.

very small annual cycle in $2CH_4 + H_2O$, of order 0.1–0.2 ppmv; see Fig. 16), an estimate of the mixing time τ may be estimated from

$$\frac{dA}{dt} = \frac{A - A_0}{\tau},$$

where A is the amplitude of the tropical annual harmonic, A_0 is the midlatitude value, and d/dt is the derivative following the upward propagating signal. This is an approximation to Eq. (1), where the meridional and eddy transport terms are approximated as a mixing process with timescale τ. Using dA/dt = (0.4 ppmv per 10 months) between 68 and 32 mb, and $(A - A_0) \sim$ (0.6 ppmv) averaged over 68–32 mb, gives an estimate of $\tau \sim 15$ months. This is a lower limit on the meridional mixing time for air entering the Tropics (30°N–S) from middle latitudes above 19 km, in order to maintain the observed tropical annual cycle. The estimate of 15 months is in reasonable agreement with that derived by Volk et al. (1996) from aircraft constituent measurements, and by Schoeberl et al. (1997) using *UARS* constituent data.

The upper stratosphere signal in Fig. 14 is dominated by a semiannual oscillation (SAO), with a much stronger amplitude during the first half of the year. This is a well-known aspect of the SAO (e.g., Dunkerton and Delisi 1988), related to stronger extratropical wave driving in the NH winter (as compared to the SH winter). Variations in H_2O echo those in CH_4, such that the total hydrogen $2CH_4 + H_2O$ is nearly constant throughout the seasonal cycle. Dynamics of the SAO is discussed further in the next section.

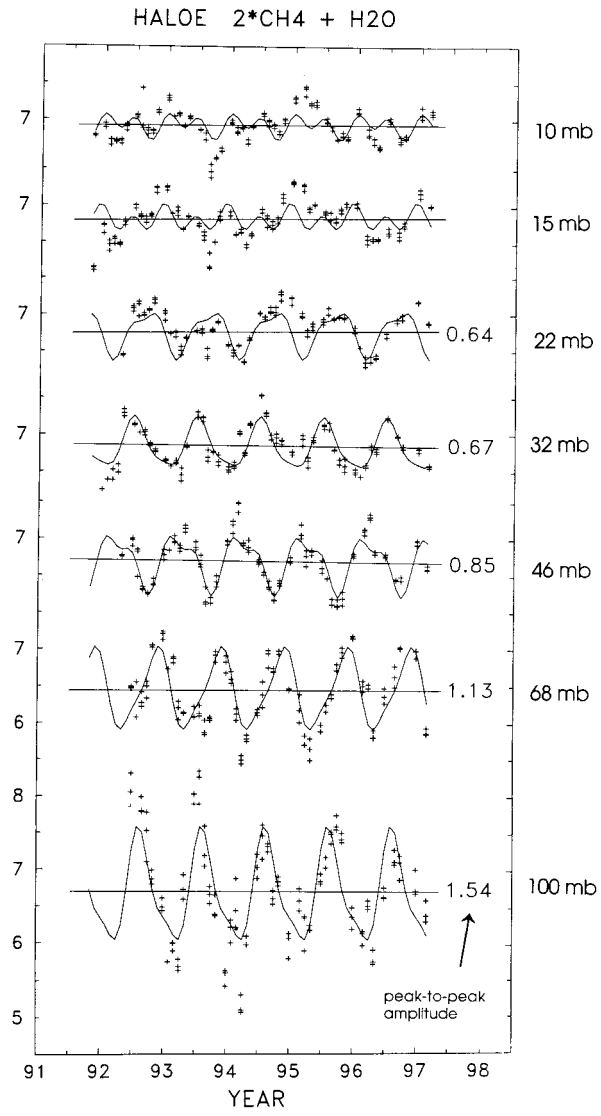

FIG. 15. Time series of $H_2O + 2CH_4$ over 4°N–4°S during 1991–97, for pressure levels 100 mb to 10 mb. Crosses show monthly means and thin lines show (repeating) seasonal cycle fits at each level.

c. Global budgets and estimates of eddy transport

In this section we examine details of the constituent continuity equation [Eq. (1)] applied to the observed seasonal cycle variations in global CH_4. For these calculations we use the monthly average residual mean circulation ($\overline{v}^*$, $\overline{w}^*$) derived from UKMO data (e.g., Fig. 10), and the chemical sink term S is approximated by a linear relaxation expression

$$\overline{S} = -\frac{\overline{\chi}}{\tau},$$

with CH_4 lifetimes (τ) taken from the model results of Garcia and Solomon (1983). The $\nabla \cdot \mathbf{M}$ term in Eq. (1) is a complicated quantity involving eddy covariances, and not derivable from the data here. We calculate this term as a residual to the balance in Eq. (1); it thus contains the actual eddy transports plus any errors in the explicitly calculated terms.

Figure 17 shows the structure of the individual terms $\partial\overline{\chi}/\partial t$, $-\overline{v}^*\overline{\chi}_y - \overline{w}^*\overline{\chi}_z$, $\overline{S}$, and $\nabla \cdot \mathbf{M}$ (calculated as a residual) for the seasonal CH_4 budget, for statistics averaged over January–February. Transport by the residual mean circulation is associated with large positive tendencies in the tropical upper stratosphere (due to upward and northward transport of relatively high CH_4) and negative tendencies over winter polar regions (due to downward transport of low CH_4). The parameterized chemical sink $\overline{S}$ is an important component of the budget in the tropical upper stratosphere, with relatively large values also over the summer (SH) high latitudes (this photochemical destruction leads to the very low CH_4 summer pole amounts observed in Fig. 11). The calculated residual ($\nabla \cdot \mathbf{M}$ term) shows a north–south dipole pattern over the Tropics and NH, with opposite sign to the mean meridional circulation transport. Although this is a residual calculation, the structure of this field shows characteristics very similar to $\nabla \cdot \mathbf{M}$ calculated explicitly using general circulation model output in Randel et al. (1994) (see their Fig. 8). An important point is that these eddy transport effects extend well into the Tropics in both model calculations and the residual estimate here. Note also that the tendency term $\partial\overline{\chi}/\partial t$ is a relatively small part of the overall budget, so that accurate simulation of $\partial\overline{\chi}/\partial t$ will be sensitive to small uncertainties in calculation of the other budget terms.

Figure 18 shows altitude–time plots of several CH_4 seasonal budget terms over the equator [$-\overline{v}^*\overline{\chi}_y$, $-\overline{w}^*\overline{\chi}_z$ and $\nabla \cdot \mathbf{M}$ (residual)]. The chemical sink S (not shown) is nearly constant over the equator throughout the year, and the observed tendency $\partial\overline{\chi}/\partial t$ (not shown) is a relatively small component. Transport by the mean meridional circulation ($\overline{v}^*$, $\overline{w}^*$) exhibits a pronounced semiannual variation in the upper stratosphere, with maxima near the solstices. Transport by both mean circulation components is important in this variation: the $\overline{w}^*$ transport is a maximum during NH winter, while the $\overline{v}^*$ component exhibits a dominant maximum during SH winter (along with a weaker NH winter peak). These enhanced $\overline{v}^*$ transports during both solstices are due to strong flow toward the winter hemisphere (see Fig. 17) combined with enhanced meridional constituent gradients near the equator (see Fig. 6). The budget residual ($\nabla \cdot \mathbf{M}$ in Fig. 18) also shows a strong semiannual variation at the equator for altitudes above approximately 30 km. Although some component of this may be due to budget uncertainties, this semiannual seasonality is consistent with enhanced planetary wave transport in the respective winter hemispheres reaching into the Tropics (as discussed above). The strong semiannual forcing (by both mean flow and eddy components) is likely responsible for the dominance of semiannual behavior for the tropical constituent fields above ~30 km (see Figs. 14 and 15).

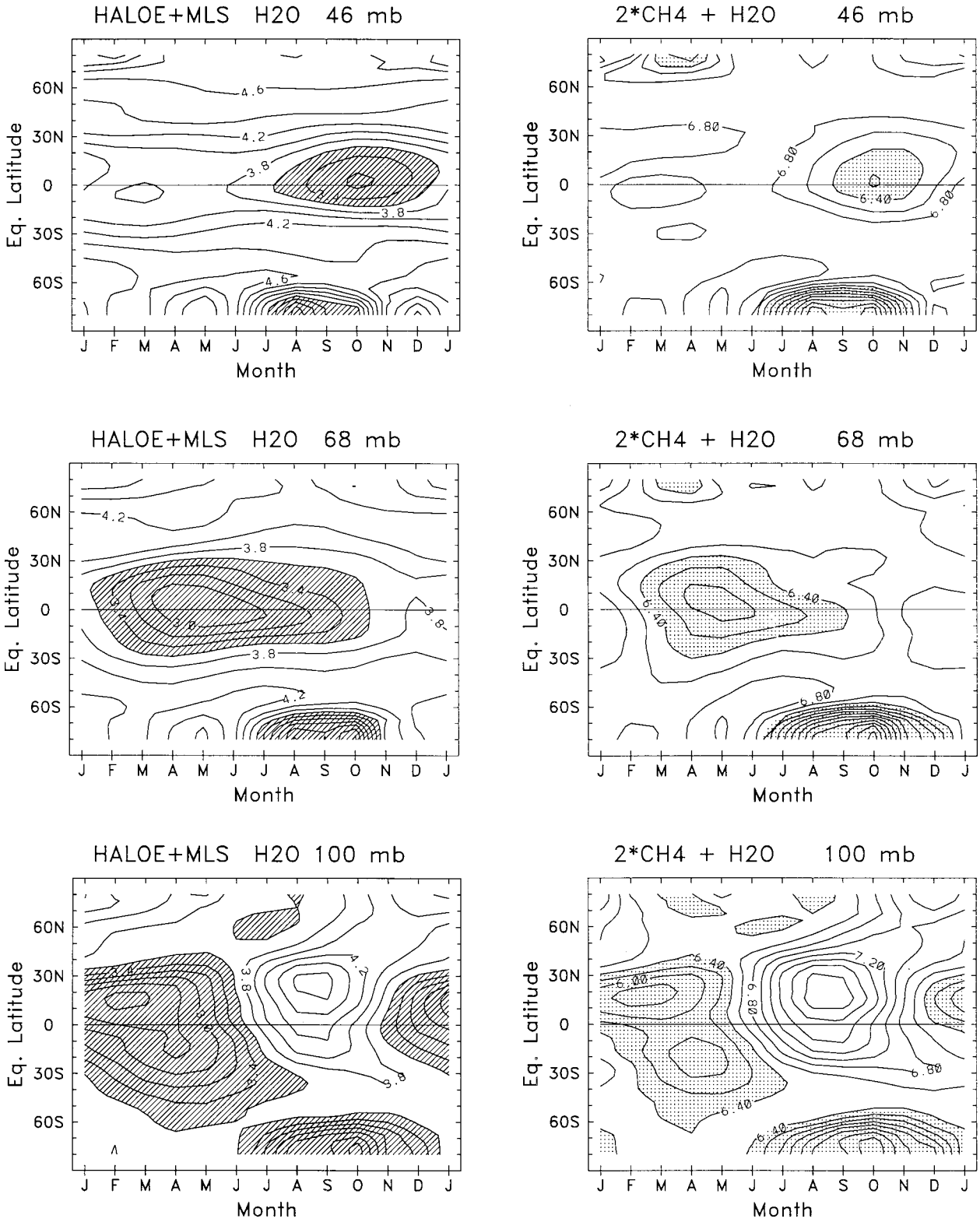

FIG. 16. Latitude–time plots of seasonality in H_2O (left) and $H_2O + 2CH_4$ (right) at 100 mb (bottom), 68 mb (middle), and 46 mb (top). Contour interval is 0.2 ppmv in each panel.

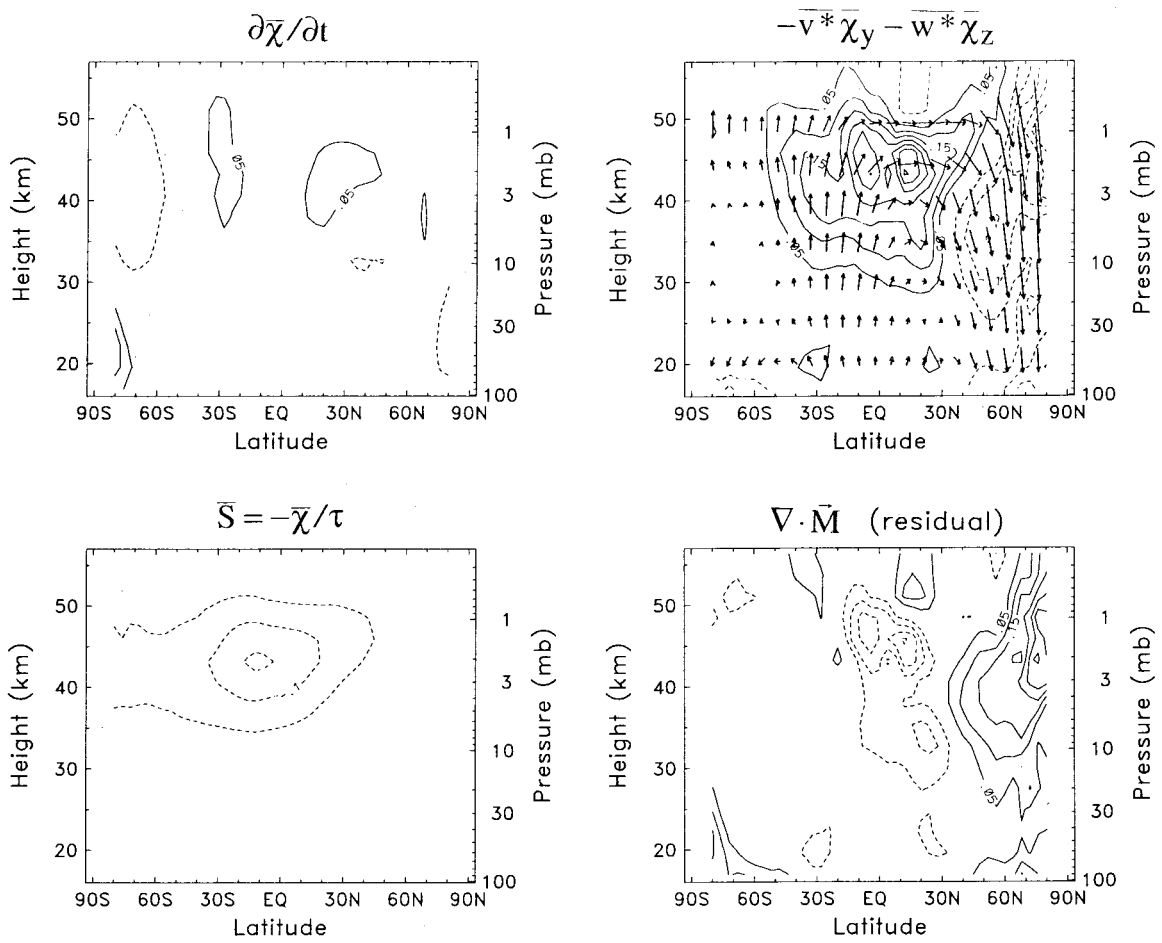

FIG. 17. Meridional cross sections of individual terms in the seasonal CH_4 continuity equation [Eq. (1)], for averages during January–February. Contour interval in all panels is 0.05 ppmv month^{-1}, with zero contours omitted. Vectors in the upper right-hand panel denote components of the residual mean circulation ($\overline{v}^*$, $\overline{w}^*$). The $\nabla\cdot\mathbf{M}$ term (lower-right panel) is calculated as a residual.

4. Interannual variability and the QBO

a. Observations

This section focuses on interannual variations in CH_4 and H_2O over 1991–97, defined as deviations from the seasonal cycles defined above (with linear trends also removed). Figure 19 shows altitude–time sections of CH_4 anomalies over the equator (average over 10°N–10°S); here data gaps have been interpolated and the monthly anomalies smoothed slightly in time. Largest CH_4 anomalies are observed in the upper stratosphere, over 35–45 km, with an approximate 2-yr periodicity; these values represent approximately ±10% deviations from the time mean. The approximate 2-yr periodicity in CH_4 anomalies suggests a link with the equatorial quasibiennial oscillation (QBO), and this is confirmed by comparison with the UKMO equatorial zonal wind anomalies shown in Fig. 20a (with the CH_4 anomalies superimposed). Specifically, the CH_4 anomalies over 35–45 km are approximately in phase with the zonal wind anomalies near 30 km.

Figure 21 shows the H_2O interannual anomalies over the equator. Maxima are observed in the upper stratosphere with very similar (but oppositely signed) patterns to the CH_4 anomalies, reflecting conservation of $2CH_4 + H_2O$ on interannual (as well as seasonal) timescales. There are also significant H_2O anomalies in the lower and middle stratosphere; there are relative maxima over 27–33 km with an approximate 2-yr periodicity, but these are not observed in the CH_4 data.

Space–time structure of coherent QBO variations in CH_4 may be isolated in an optimal manner using singular value decomposition (SVD) (Randel and Wu 1996). This involves manipulation of the covariance matrix between CH_4 anomalies (as a function of latitude and altitude) and zonal wind anomalies (over 10–70 mb), and yields modal spatial structures that explain optimum fractions of covariance between these fields. Figure 22 shows the spatial structure of the first two modes derived from this analysis (termed SVD1 and SVD2); patterns show the location (and phase) of anomalies in CH_4 that are coherent with the QBO zonal wind

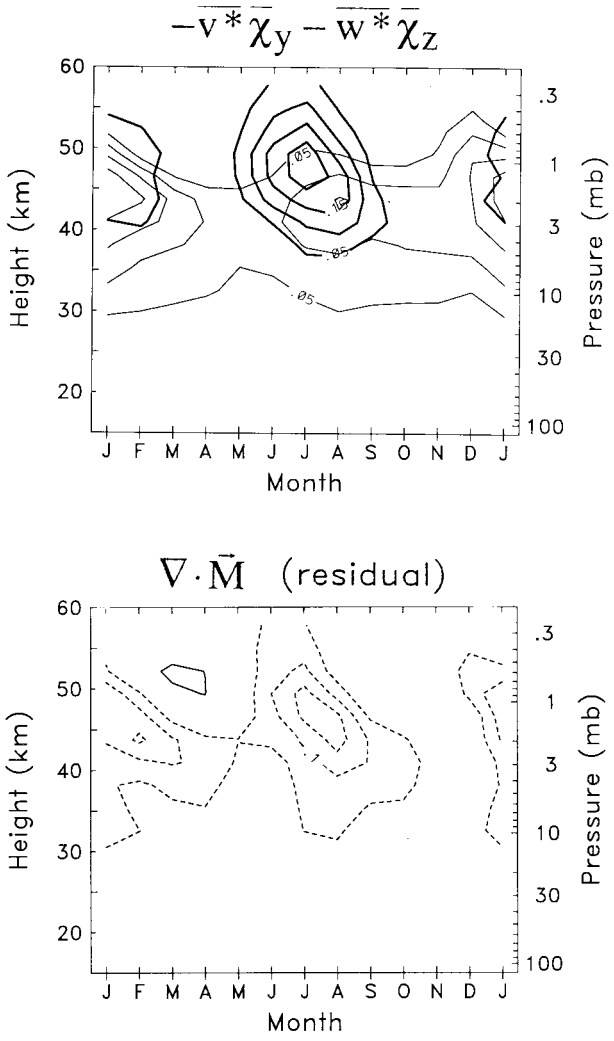

FIG. 18. Altitude–time sections of terms in the seasonal CH_4 continuity equation [Eq. (1)] over the equator. Shown are $-\overline{v^*}\overline{\chi_y}$ (top panel, heavy lines), $-\overline{w^*}\overline{\chi_z}$ (top panel, light lines), and $\nabla \cdot \mathbf{M}$ (calculated as a residual—bottom panel). Contour interval in both panels is 0.05 ppmv month^{-1}, with zero contours omitted.

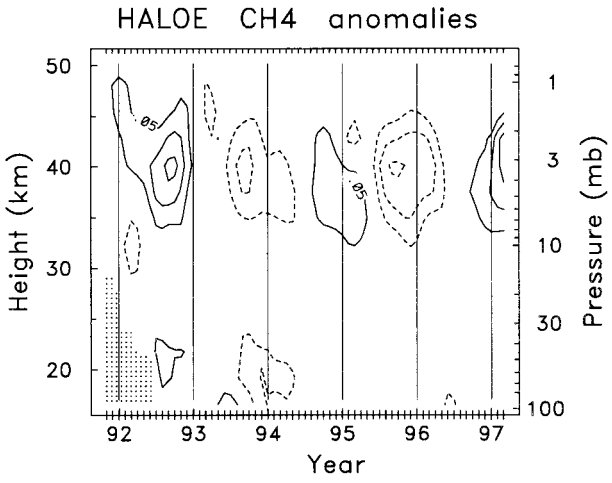

FIG. 19. Altitude–time section of interannual anomalies in CH_4 over the equator. Contour interval is 0.05 ppmv, with zero contours omitted. The vertical lines denote January for each year.

anomalies. (Two such modes are typical for a propagating oscillation, analogous to a harmonic sine and cosine Fourier decomposition.) The spatial structure of SVD1 shows a maximum in the upper stratosphere over 35–45 km, centered in the Tropics over approximately 30°N–S. This structure corresponds to the equatorial anomalies seen in Fig. 19. The structure of SVD2 shows a narrow maximum over the equator at 40–45 km, and several maxima over ~10°–40° in both hemispheres [note these modes are spatially (and temporally) orthogonal by construction]. These extratropical patterns are qualitatively similar to QBO variations observed in column and profile ozone and NO_2 data (Bowman 1989; Randel and Wu 1996), and deduced from CLAES N_2O data by O'Sullivan and Dunkerton (1997). The QBO patterns in Fig. 22 are largest near gradients in the background CH_4 structure (included in Fig. 22), as anticipated for anomalies due to transport variations. Note the similarity of these QBO patterns with the total interannual variance map shown in Fig. 5.

Temporal evolution of the QBO patterns in CH_4 is revealed by projection of the full monthly CH_4 anomalies onto the spatial patterns in Fig. 22. Figure 23 shows a phase-space plot of the projections of SVD1 versus SVD2 over the entire time record 1991–97. Nearly regular counterclockwise phase progression is observed as the QBO anomalies project successively onto the patterns in Fig. 22. This nearly regular QBO phase variation in CH_4 data is analogous to the harmonic QBO variations in dynamical quantities discussed by Wallace et al. (1993), and the ozone variations shown in Randel and Wu (1996).

Figure 24 shows CH_4 data observed during April for four years (1993–96); these time periods are indicated in Fig. 23 and correspond to opposing projections of SVD1 and SVD2. These plots demonstrate that there is a strong effect of the QBO in modulating the double-peaked structure in upper-stratospheric CH_4: data during April 1993 and 1995 (westerly QBO winds in Fig. 20a) exhibit a pronounced double peak, whereas April 1994 and 1996 (easterly QBO winds) do not.

Figure 25 shows latitude–time series at 3 mb of the full CH_4 field and the detrended anomalies (which exhibit a clear QBO dependence). Time periods of enhanced double-peak structure are also indicated in Fig. 25. The QBO anomalies show maxima centered near the equator, with a suggestion of propagation into the subtropics, particularly into the NH. This latitudinal propagation near 3 mb is associated with successive projections of SVD1 and SVD2 (Fig. 22). The timing of these anomalies is such that large NH subtropical maxima occur during NH winter–spring; this is the time of seasonal maximum in SH subtropics, and this com-

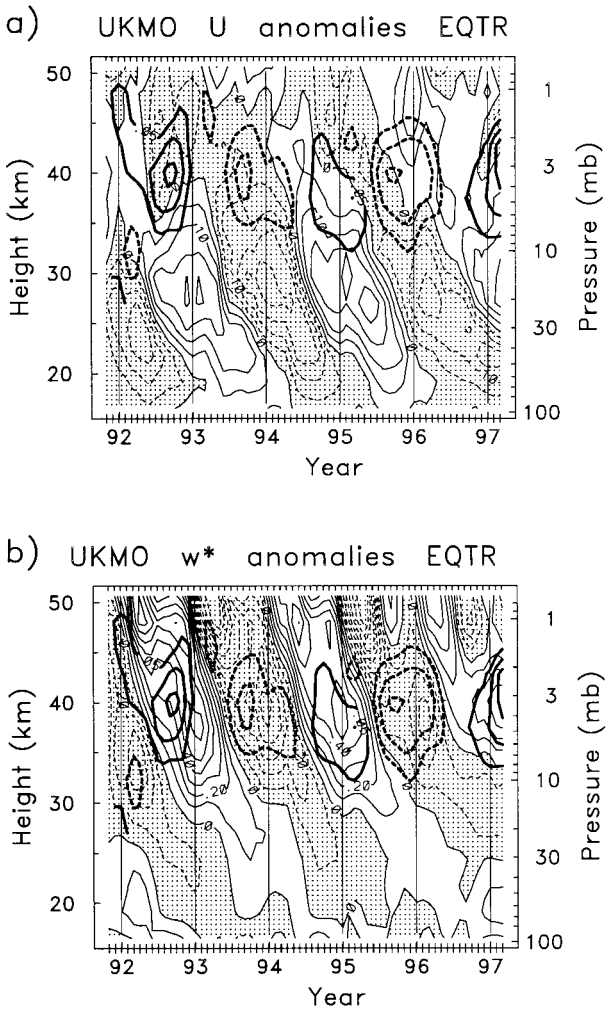

FIG. 20. Altitude–time sections of interannual anomalies in (a) zonal-mean zonal wind and (b) QBO-filtered vertical velocity $\overline{w^*}$ over the equator, derived from UKMO analyses. Contour interval is 5 m s^{-1} and 0.1 km $month^{-1}$, respectively. Heavy contours near 40 km are CH_4 anomaly isolines (from Fig. 19).

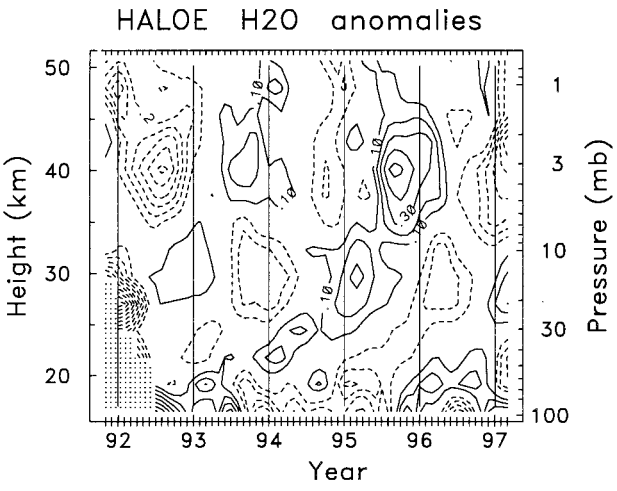

FIG. 21. Altitude–time sections of interannual anomalies in H_2O over the equator. Contour interval is 0.1 ppmv, and zero contours are omitted.

bination leads to double-peaked structure for the positive QBO anomalies in NH spring 1993 and 1995. The details of this behavior clearly depend on the phase relationship between the QBO and the seasonal cycle, and this is something that will change on a decadal timescale (Gray and Dunkerton 1990). We note that relatively small anomalies are observed over the equator during these times; the double-peak structure (or its absence) in this time sample is mostly due to the presence of subtropical anomalies, particularly in the NH (corresponding to a positive projection of SVD1 + SVD2, i.e., Fig. 23).

Figure 26 shows the latitude–time evolution of CH_4 at 10 mb throughout 1991–97, for both the full-field and interannual anomalies. The anomalies at this altitude are very small at the equator but large over the subtropics of each hemisphere (somewhat larger in the NH), with a strong QBO time dependence. These interannual anomalies are associated with a latitudinal shifting of the tropical maximum region in CH_4, as seen in the upper panel of Fig. 26. The maximum is shifted toward the NH during QBO easterlies (near 30 mb) enhancing NH subtropical gradients, and toward the SH for QBO westerlies (decreasing these gradients). Similar CH_4 patterns are observed over approximately 22–10 mb (27–32 km), but not below 30 mb; these anomalies are associated with strong projection onto SVD2 in Fig. 22. Note the clear effect of these anomalies in the cross sections in Fig. 24, especially on the vertical gradient structure in NH midlatitudes. This is remarkable evidence of QBO modulation of the latitudinal position of the tropical maximum region (Trepte and Hitchman 1992) and the interaction with extratropics.

Figure 27 shows the latitudinal structure of H_2O at 10 mb throughout 1991–97, for both the full field and the interannual anomalies. Large anomalies are observed in the NH subtropics, mirroring the CH_4 patterns in Fig. 26. Unlike the CH_4 data, the H_2O anomalies extend across the equator, giving rise to the equatorial anomalies centered near 10 mb seen in Fig. 21. The overall structure of H_2O at 10 mb shows latitudinal movement of the tropical minimum region and modulation of subtropical gradients on the QBO timescale, very similar to that seen for CH_4 in Fig. 26.

b. QBO budget calculations

The observed QBO anomalies in CH_4 and H_2O likely result from transport variations associated with the QBO. Although a detailed budget analysis of QBO transport is beyond the scope of this work, there are some aspects of coupling with QBO circulation anomalies that deserve mention. Figure 20b shows an altitude–time section of the QBO anomalies in residual mean vertical velocity ($\overline{w^*}$) over the equator derived from UKMO data (Randel

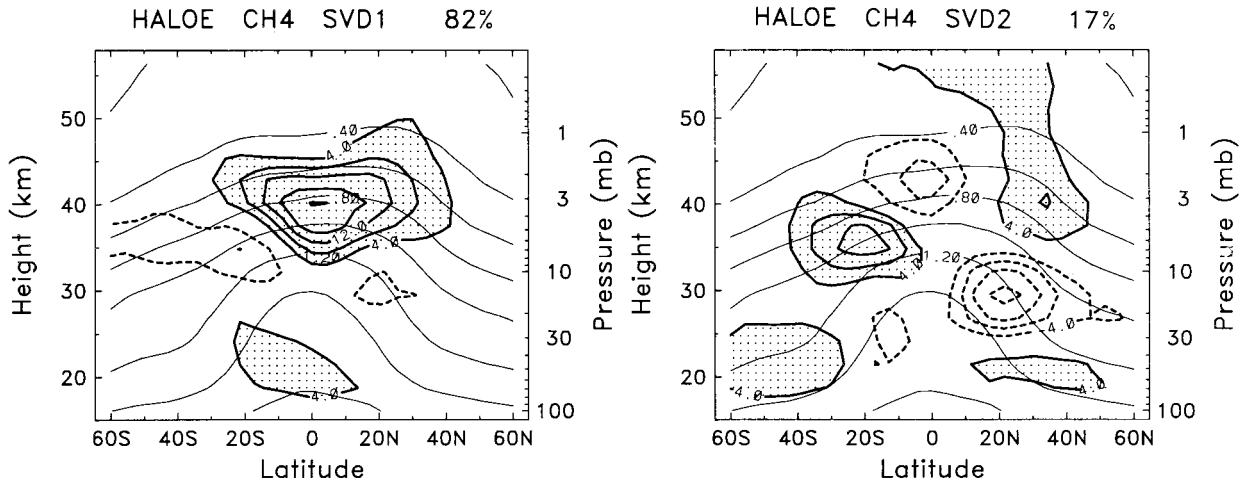

FIG. 22. Heavy solid and dashed lines with shading show the spatial structure of QBO SVD1 (left) and SVD2 (right) for CH_4. Contours show local mixing ratio variations with arbitrary units. Light lines denote background annual mean CH_4 structure.

et al. 1997). These data have been filtered to isolate QBO variations, but the QBO patterns are clearly evident in the full interannual anomaly fields (see W. Randel et al. 1998, manuscript submitted to *J. Atmos. Sci.*). These $\overline{w^*}$ anomalies are maximum near regions of largest vertical shear of the zonal-mean wind (Fig. 20a)—which are also regions of largest QBO temperature anomalies—and exhibit similar downward propagation in time. These QBO anomalies in $\overline{w^*}$ are of order 10%–20% of the time-mean background values; largest $\overline{w^*}$ anomalies are observed in the upper stratosphere (35–45 km), although largest QBO zonal winds are seen in the lower-middle stratosphere. Comparison between the vertical velocity anomalies and the equatorial CH_4 anomalies (also included in Fig. 20b) shows strong correlation in the upper stratosphere, with upward velocities associated with positive CH_4 maxima, and vice versa.

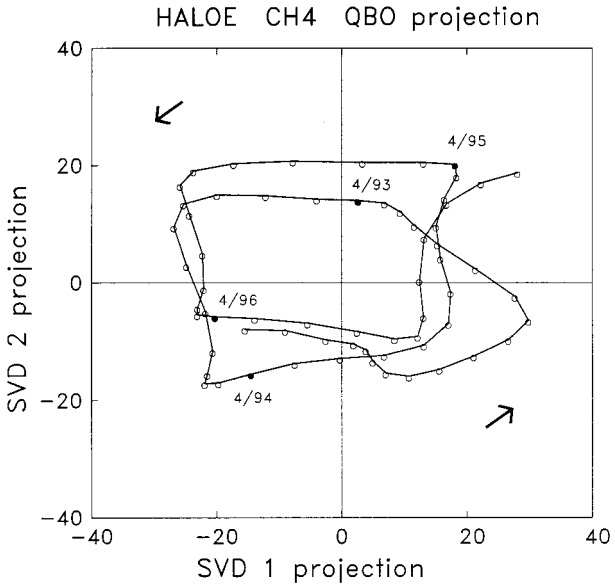

FIG. 23. Phase–space diagram of the projection of the monthly global CH_4 anomalies onto spatial structures SVD1 and SVD2 (shown in Fig. 22). Time progression corresponds to counterclockwise orbit transits, with locations during several months noted.

The observed space–time coherence between QBO anomalies in $\overline{w^*}$ and CH_4 in the equatorial upper stratosphere (Fig. 20b) is puzzling in light of Eq. (1). If vertical transport is the dominant effect (a reasonable assumption for equatorial QBO variations), the continuity equation [Eq. (1)] suggests a correlation between $\overline{w^*}$ and $\partial\overline{\chi}/\partial t$, rather than between $\overline{w^*}$ and $\overline{\chi}$ as observed. An estimate of the budget based on Eq. (1) (not shown) results in large residuals with an approximate QBO periodicity, with a phase relationship such that the residual is a (negative) maximum during QBO westerly winds. One possible explanation is that eddy transport effects are modulated by the QBO zonal wind structure. Although this is speculative, based on variations in the residual to Eq. (1), the in-phase coherence between $\overline{w^*}$ and CH_4 (or H_2O) anomalies near 40 km appears to be a robust result (leading to these large residuals).

Figure 28 shows a latitude–time diagram of the QBO anomalies in $\overline{w^*}$ at 10 mb. Together with alternating anomalies over the equator (over 10°N–S), this figure shows large anomalies in the NH subtropics that are approximately out of phase with those at the equator. These coupled patterns are likely a manifestation of the meridional circulation cells anticipated theoretically for the QBO (e.g., Plumb and Bell 1982), although the meridional scale is somewhat wider than in idealized models and there is substantial NH–SH asymmetry in these observations. The subtropical $\overline{w^*}$ maxima at 10 mb bear strong resemblance to the CH_4 and H_2O anomaly patterns shown in Figs. 26 and 27. Comparison of the time evolution shows the circulation anomalies lead the constituent patterns by up to a quarter cycle (as expected for transport variations), al-

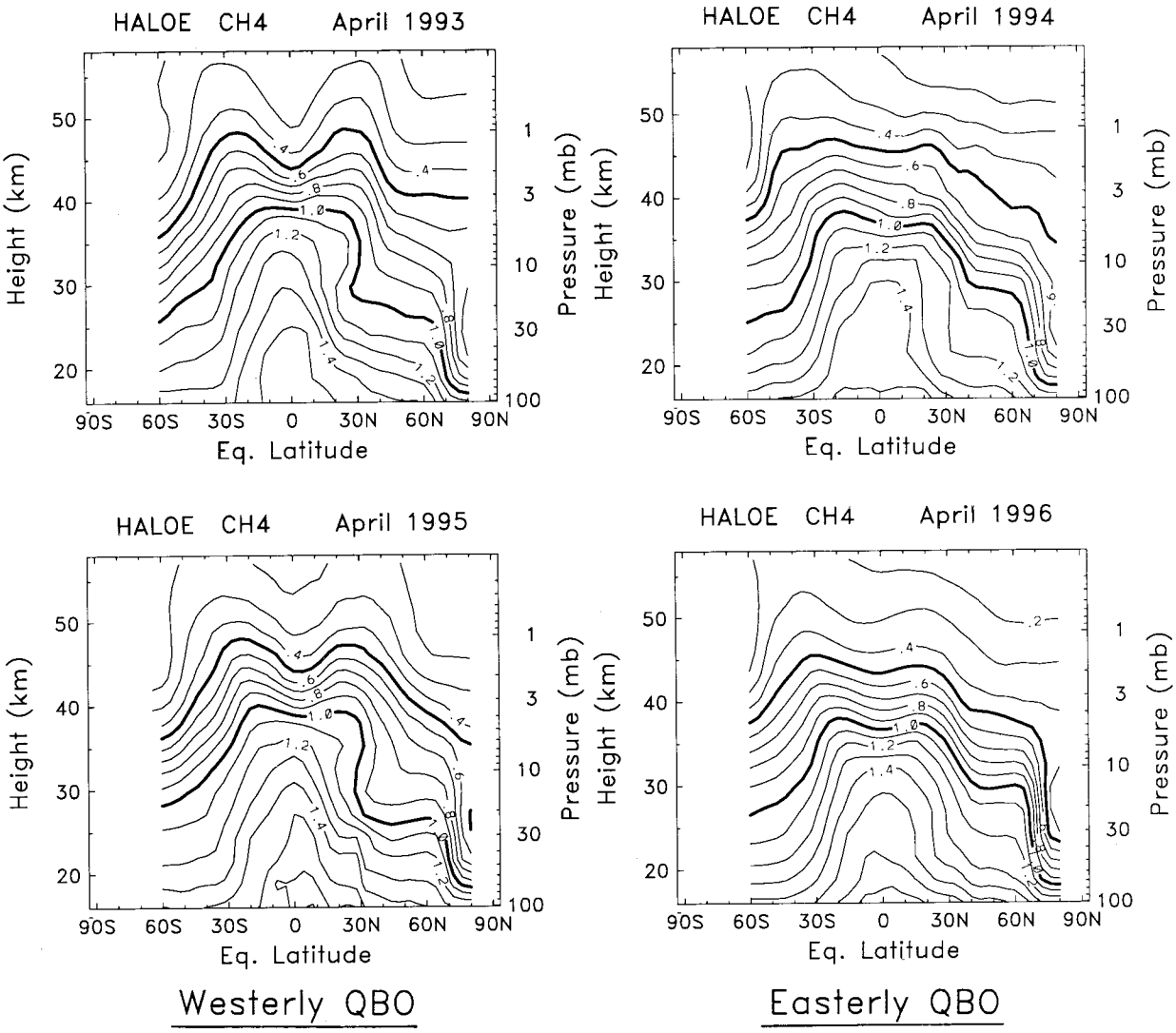

FIG. 24. Meridional cross sections of CH_4 during April 1993, 1994, 1995, and 1996 (time periods denoted in Fig. 23). Note the double-peaked upper stratosphere patterns in 1993 and 1995.

though the anomalies in early 1994 are more nearly in phase. The similarity in these patterns suggests that advection by the mean meridional circulation is one important component for forcing the observed subtropical QBO constituent variations. Model calculations furthermore suggest that eddy transport effects are important for modulation of the subtropical mixing barrier (Polvani et al. 1995; O'Sullivan and Chen 1996).

5. Summary and discussion

High quality observations of stratospheric CH_4 and H_2O from HALOE provide a near-continuous global record of seasonal and interannual variations in stratospheric transport. Motivated by the observed strong correlation between these tracers and derived potential vorticity (PV) fields, we have mapped the HALOE data into equivalent latitude (PV) coordinates. This has the dual advantages of separating physically distinct measurements and increasing the effective latitude sampling of the data (see Fig. 2). Seasonal cycles are then constructed by harmonic regression analysis of monthly binned data. To obtain complete global seasonal cycles, we have included CLAES CH_4 and MLS H_2O data over polar winter regions (with smooth transitions obtained by matching the data over midlatitudes). These global seasonal cycle data allow novel study of details in the seasonal cycle of stratospheric transport. These data will also be useful for initializing or studying transport characteristics in stratospheric models.[1]

[1] These seasonal cycle datasets (and similar ones for other HALOE constituents) are available to potential users via anonymous FTP from NCAR (contact the author at randel@ucar.edu).

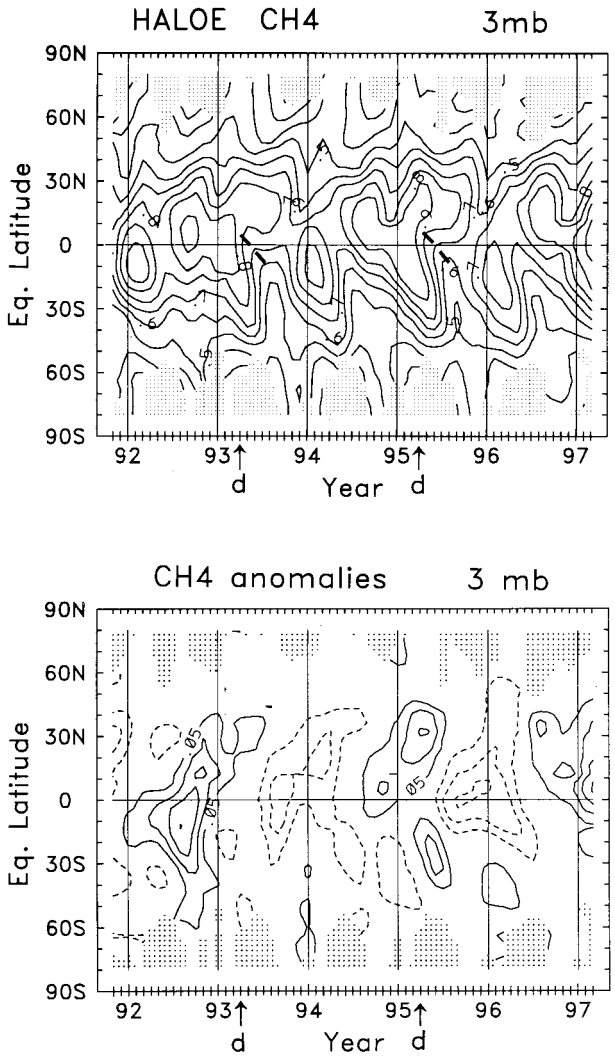

FIG. 25. Latitude–time sections of CH_4 at 3 mb during 1991–97. Shown are the full field (top) and the detrended interannual anomalies (bottom). Dashed lines and arrows denote periods of double-peaked (d) latitudinal structure.

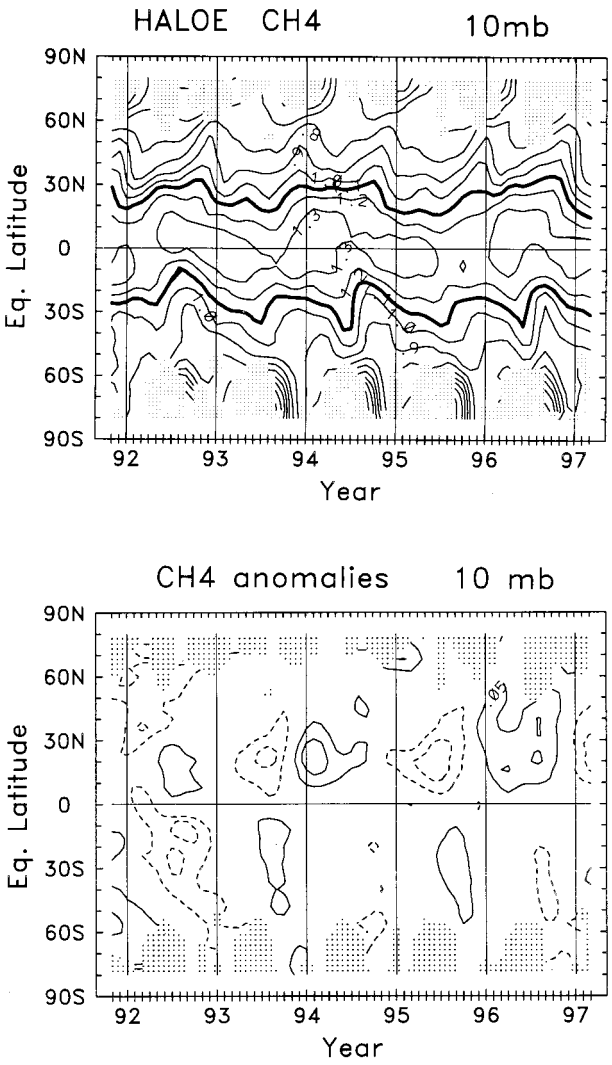

FIG. 26. Latitude–time sections of CH_4 at 10 mb over 1991–97, for the full field (top—contour interval 0.1 ppmv) and interannual anomalies (bottom—contour interval of 0.05 ppmv, with zero contours omitted).

The seasonal cycle of CH_4 in the lower stratosphere shows characteristics that have similar space–time structure to vertical velocity fields derived from meteorological analyses. This is a reasonable finding, as CH_4 is strongly vertically stratified. The enhanced subtropical gradients observed in CH_4 coincide with the region of weak vertical motions, that is, where the tropical upwelling changes to middle–high-latitude downward motion. Furthermore, a seasonal latitudinal shifting of both the tropical CH_4 and vertical velocity fields is observed, with isolines displaced slightly into the respective summer hemispheres. This behavior suggests that tropical upwelling plays a large role in formation of the subtropical gradients for tropospheric source gases; winter hemisphere wave activity is also likely to be important (Polvani et al. 1995; Waugh 1996).

Polar regions in the lower stratosphere of both hemispheres show very similar seasonality in CH_4, with very low values during spring (March–April in the NH and October–November in the SH). Such low values in the SH vortex have been discussed by Russell et al. (1993a) and Schoeberl et al. (1995) and provide evidence of relatively unmixed descent from high altitudes. The similar low values observed in the NH data here are due to having organized the observations according to the polar vortex structure (i.e., zonal means do not show such low values). Good agreement with vertical transport calculations (Fig. 12) confirms isolation of the SH polar vortex and demonstrates that the vertical velocities (derived primarily from radiative heating codes) are reasonably correct. Poor agreement in the NH (Fig. 13) suggests less isolation of the NH polar vortex.

The harmonic seasonal cycle fits of the HALOE water

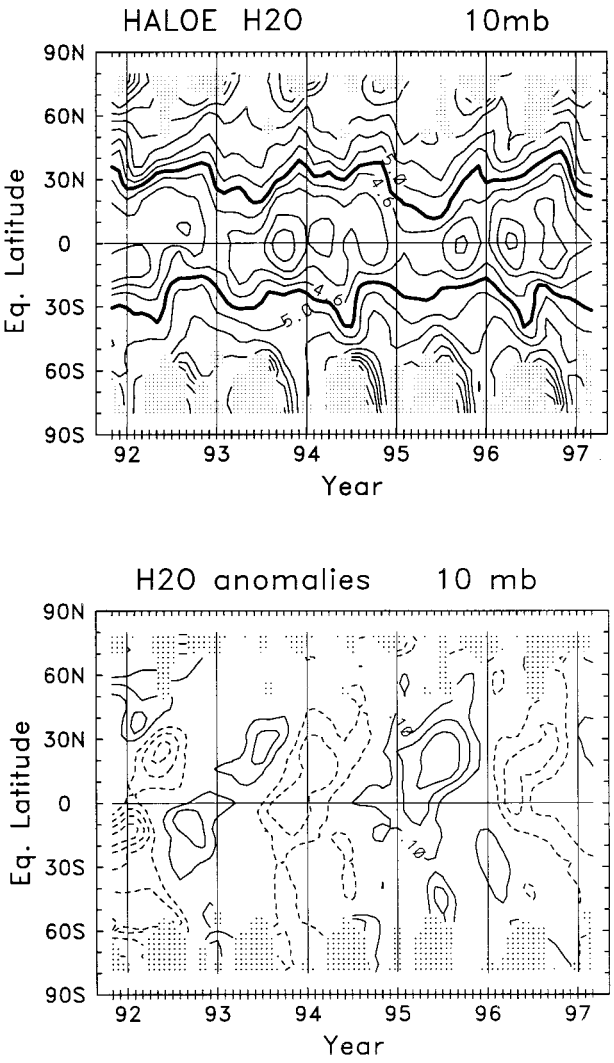

FIG. 27. Latitude–time sections of H_2O at 10 mb over 1991–97, for the full field (top—contour interval 0.2 ppmv) and interannual anomalies (bottom—contour interval of 0.1 ppmv, with zero contours omitted).

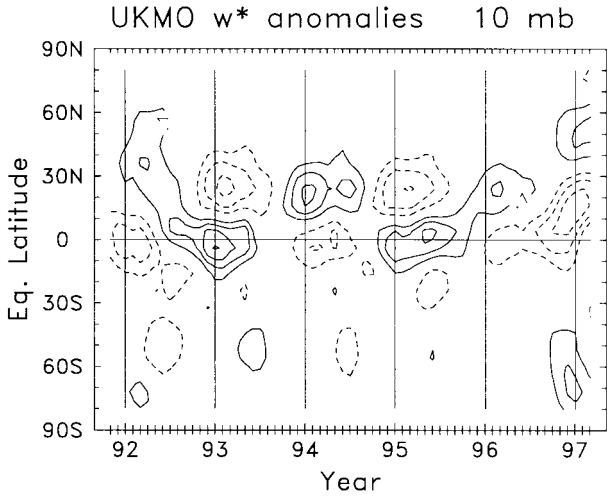

FIG. 28. Latitude–time section of interannual anomalies in TEM vertical velocity ($\overline{w^*}$) at 10 mb. These data have been filtered to isolate components coherent with the zonal wind QBO, and multiplied by cos (latitude) to accentuate tropical features. Contour interval is 0.1 km month^{-1}, with zero contours omitted.

vapor data provide a clear view of the upward-propagating annual cycle in the Tropics (Figs. 15–17). The annual cycle is dominant over 100–22 mb (up to ~27 km); above this altitude the seasonal variation is primarily semiannual. The lack of propagation of the annual cycle above 27 km suggests there is somewhat stronger horizontal mixing above this altitude, with less isolation of tropical air (i.e., this is the upper level of the tropical ''reservoir''). This is consistent with enhanced tropical mixing above 10 mb noted by Dunkerton and O'Sullivan (1996). Two mechanisms for enhanced mixing with a semiannual timescale are 1) mean circulation advection, and 2) the tropical extension of winter hemisphere planetary wave effects.

The annual cycle in water vapor at and above 68 mb is centered over the equator, whereas seasonality at 100 mb shows relative maxima in the NH subtropics. Regions of high H_2O at 100 mb during NH summer are particularly shifted toward the NH, and there is evidence of strong transport into NH middle and high latitudes (Fig. 16). The asymmetry of these patterns (both in location of the tropical extrema and the latitudinal propagation) contributes to a significantly wetter lower stratosphere in the NH compared to the SH (Kelly et al. 1990; RO97). There is little meridional spreading of the tropical annual cycle above 68 mb beyond 30°N–S; the slow weakening of the tropical annual cycle with altitude over 68–22 mb is further evidence of tropical isolation, and these data infer an exchange time of order 15 months for mixing of midlatitude air into the Tropics. These data also demonstrate that there is little influence of Antarctic dehydration in SH midlatitudes following vortex breakup (as also noted from the analyses of RO97).

The data here show strong seasonality in the tropical upper stratosphere, for both CH_4 and H_2O, with the characteristics of a semiannual cycle forced by alternating upwelling in the respective summer subtropics. This semiannual signal in H_2O was also discussed by McCormick et al. (1993) and Eluszkiewicz et al. (1996). A double-peaked latitudinal structure is evident in the climatology during April–June, but this is strongly modulated by the phase of the QBO.

A global budget analysis of the seasonal cycle CH_4 data using UKMO residual mean circulation estimates and parameterized photochemical loss rates showed large residuals, which we attribute (at least in part) to eddy transport effects. The patterns of these eddy transport tendencies show a north–south dipole pattern, with positive tendencies in the winter stratosphere and negative tendencies in low latitudes (extending across the

equator). These eddy transports, which are derived as a residual here, are very similar to the explicit eddy transport calculations performed using general circulation model output in Randel et al. (1994). Other studies have also suggested that the effects of planetary waves reach low latitudes (Polvani et al. 1995; Waugh et al. 1996; O'Sullivan 1997). There is a clear semiannual variation of the eddy transports (residuals) in the Tropics, and this is consistent with the amplification of large-scale wave transports in the respective winter hemispheres.

A number of model and diagnostic studies have been used in an attempt to explain the double-peaked constituent patterns in the tropical upper stratosphere (e.g., the April patterns in Figs. 6 and 7) (Gray and Pyle 1986, 1987; Hamilton and Mahlman 1988; Choi and Holton 1991; Sassi et al. 1993; Kennaugh et al. 1997). The mechanism for the double peak in these studies is downward motion over the equator (associated with the westerly shear zone of the dynamical SAO during equinox) coupled with upward motion in subtropics. A common feature of these studies, however, is an underestimation of the strength of the double peak, which is usually attributed to a lack of resolved downward motion over the equator. However, the balance of terms in the budget analyses here suggests that the vertical mean circulation does not primarily determine the tropical behavior. Transport by the $\overline{v}^*$ circulation contributes large positive SAO tendencies in the tropical upper stratosphere during both solstices, due to strong flow toward the winter hemisphere and enhanced meridional constituent gradients near the equator. Chemical relaxation is a relatively large budget component, but exhibits little seasonality in the Tropics. There are also relatively large residuals in the tropical budget during solstice seasons, and these may be at least partly attributable to winter hemisphere eddy transport effects that reach the Tropics.

A majority of the interannual variance over the 1991–97 time sample analyzed here is found to be coherent with the QBO; aspects of QBO variations in HALOE CH_4 have also been shown in Luo et al. (1997) and Ruth et al. (1997). The structure of the QBO signal in CH_4 exhibits a maximum in the tropical upper stratosphere over 35–45 km. This is somewhat higher than the QBO signals observed in ozone (~20–38 km) and nitrogen dioxide (~28–35 km) (Zawodny and McCormick 1991). These differing vertical structures are attributable to differences in the respective background means (e.g., Chipperfield and Gray 1992); the strongest background gradients in CH_4 are observed over 35–45 km.

We find that the QBO exerts a strong influence on appearance of the double-peaked ''rabbit ears'' structure in the tropical upper stratosphere during NH spring: the double peak occurs primarily when QBO westerlies are present near 10 mb. The double-peaked structure in the mean seasonal cycle (Figs. 6 and 7) represents a time average over both phases of the QBO. This has implications for numerical simulation of the stratopause SAO and its effects on tracer distributions (e.g., Sassi et al. 1993), suggesting that details of the winds in the lower stratosphere may be important. Kennaugh et al. (1997) have recently presented a modeling study of this QBO influence on the double peak.

The observed equatorial CH_4 (and H_2O) QBO anomalies over 35–45 km are observed to be strongly correlated with anomalies in the residual mean vertical circulation $\overline{w}^*$ (Fig. 20b). This is a curious result in light of the anticipated dominance of vertical transport in this region, as the continuity equation [Eq. (1)] suggests a correlation between $\overline{w}^*$ and $\partial\chi/\partial t$ (not $\overline{\chi}$). Budget calculations show a large residual with a QBO periodicity, and one possible explanation is that eddy transports in the tropical upper stratosphere are modulated by QBO winds (with maximum negative tendencies during QBO westerly winds). This is not unreasonable in light of observational (Dunkerton and Baldwin 1991; Baldwin and Dunkerton 1991) and modeling (O'Sullivan and Chen 1996) studies showing QBO modulation of planetary wave effects in both subtropics and midlatitudes.

These constituent data also show evidence of a latitudinal shifting of the tropical maximum region and modulation of subtropical gradients in the middle stratosphere (~27–32 km) associated with the QBO. There is a shift of approximately 10°–15° lat correlated with the QBO winds near 30 mb, with movement toward the NH during QBO westerlies. The sharpening of the NH subtropical gradients during QBO easterlies is similar to the patterns observed in stratospheric aerosol by Hitchman et al. (1994) and Grant et al. (1996). Examination of QBO anomalies in $\overline{w}^*$ at 10 mb shows relatively large subtropical maxima that are approximately in quadrature with the constituent anomalies, suggesting that advection by the mean circulation may be important [presumably in addition to eddy transports, e.g., Polvani et al. (1995) and O'Sullivan and Chen (1996)]. One caveat to interpretation of the QBO results here is that there is a certain phasing of the QBO and seasonal cycle for this relatively short record (~ two QBO cycles); details of the QBO in constituent transport may evolve as this phase relationship changes slowly in time. Overall there is reasonable agreement between the space–time patterns of QBO variations in CH_4 and H_2O throughout the stratosphere. One region of apparent difference is over the equator near 10 mb, where anomalies are seen in H_2O but not CH_4. Details of these differences await explanation.

Acknowledgments. Much of the work reported here was completed while WJR was on sabbatical at the Cooperative Research Center for Southern Hemisphere Meteorology at Monash University, Australia. We thank Tim Hall and Darryn Waugh for many useful discussions throughout the course of this work, particularly regarding tropical transport. We thank K.-K. Tung for providing the radiative heating code, and Barbara Naujokat for updated QBO winds. Dan Packman and Charles Cavanaugh managed the *UARS* data archive at

NCAR. We thank Rolando Garcia, Boris Khattatov, and Mark Schoeberl for discussions and comments on the manuscript and Lesley Gray and Phil Mote for constructive and helpful reviews. Marilena Stone expertly prepared the manuscript. This work was partially supported under NASA Grants W-18181 and W-16215. The National Center for Atmospheric Research is sponsored by the National Science Foundation.

REFERENCES

Andrews, D. G., J. R. Holton, and C. B. Leovy, 1987: *Middle Atmosphere Dynamics.* Academic Press, 489, pp.

Bacmeister, J. T., M. R. Schoeberl, M. E. Summers, J. R. Rosenfield, and X. Zhu, 1995: Descent of long-lived trace gasses into the winter polar vortex. *J. Geophys. Res.,* **100,** 11 669–11 684.

Baldwin, M. P., and T. J. Dunkerton, 1991: Quasi-biennial oscillation above 10 mb. *Geophys. Res. Lett.,* **18,** 1205–1208.

Bithell, M., L. J. Gray, J. E. Harries, J. M. Russell, and A. F. Tuck, 1994: On the synoptic interpretation of HALOE measurements using PV analysis. *J. Atmos. Sci.,* **51,** 2942–2956.

Bowman, K. P., 1989: Global patterns of the quasi-biennial oscillation in total ozone. *J. Atmos. Sci.,* **46,** 3328–3343.

——, 1993: Large-scale isentropic mixing properties of the Antarctic polar vortex from analyzed winds. *J. Geophys. Res.,* **98,** 23 013–23 027.

Brewer, A. W., 1949: Evidence for a world circulation provided by measurements of helium and water vapor distribution in the stratosphere. *Quart. J. Roy. Meteor. Soc.,* **75,** 351–363.

Buchart, N., and E. E. Remsberg, 1986: The area of the stratospheric polar vortex as a diagnostic for tracer transport on isentropic surfaces. *J. Atmos. Sci.,* **43,** 1379–1405.

Chen, P., J. R. Holton, A. O'Neill, and R. Swinbank, 1994: Quasi-horizontal transport and mixing in the Antarctic stratosphere. *J. Geophys. Res.,* **99,** 16 851–16 855.

Chipperfield, M. P., and L. J. Gray, 1992: Two dimensional model studies of the interannual variability of trace gasses in the middle atmosphere. *J. Geophys. Res.,* **97,** 5963–5980.

Choi, W.-K., and J. R. Holton, 1991: Transport of N_2O in the stratosphere related to the equatorial semiannual oscillation. *J. Geophys. Res.,* **96,** 22 543–22 557.

Dessler, A. E., E. M. Weinstock, E. J. Hintsa, J. G. Anderson, C. R. Webster, R. D. May, J. W. Elkins, and G. S. Dutton, 1994: An examination of the total hydrogen budget of the lower stratosphere. *Geophys. Res. Lett.,* **21,** 2563–2566.

Dunkerton, T. J., and D. P. Delisi, 1988: Seasonal variation of the semiannual oscillation. *J. Atmos. Sci.,* **45,** 2772–2787.

——, and M. P. Baldwin, 1991: Quasi-biennial modulation of planetary wave fluxes in the Northern Hemisphere winter. *J. Atmos. Sci.,* **48,** 1043–1061.

——, and D. O'Sullivan, 1996: Mixing zone in the tropical stratosphere above 10 mb. *Geophys. Res. Lett.,* **23,** 2497–2500.

Eluszkiewicz, J., and Coauthors, 1996: Residual circulation in the stratosphere and lower mesosphere as diagnosed from Microwave Limb Sounder data. *J. Atmos. Sci.,* **53,** 217–240.

Fisher, M., and A. O'Neill, 1993: Rapid descent of mesospheric air into the stratospheric polar vortex. *Geophys. Res. Lett.,* **20,** 1267–1270.

Garcia, R. R., and S. Solomon, 1983: A numerical model of the zonally averaged dynamical and chemical structure of the middle atmosphere. *J. Geophys. Res.,* **88,** 1379–1400.

——, and ——, 1994: A new numerical model of the middle atmosphere 2. Ozone and related species. *J. Geophys. Res.,* **99,** 12 937–12 951.

Gille, J. C., L. V. Lyjak, and A. K. Smith, 1987: The global residual mean circulation in the middle atmosphere for the northern winter period. *J. Atmos. Sci.,* **44,** 1437–1452.

Grant, W. B., and Coauthors, 1994: Aerosol-associated changes in tropical stratospheric ozone following the eruption of Mount Pinatubo. *J. Geophys. Res.,* **99,** 8197–8211.

——, E. V. Browell, C. S. Long, L. L. Stowe, R. G. Grainger, and A. Lambert, 1996: Use of volcanic aerosols to study the tropical stratospheric reservoir. *J. Geophys. Res.,* **101,** 3973–3988.

Gray, L. J., and J. A. Pyle, 1986: The semi-annual oscillation and equatorial tracer distributions. *Quart. J. Roy. Meteor. Soc.,* **112,** 387–407.

——, and ——, 1987: Two dimensional model studies of equatorial dynamics and tracer distributions. *Quart. J. Roy. Meteor. Soc.,* **113,** 635–651.

——, and T. J. Dunkerton, 1990: The role of the seasonal cycle in the quasi-biennial oscillation of ozone. *J. Atmos. Sci.,* **47,** 2429–2451.

Hamilton, K., and J. D. Mahlman, 1988: General circulation model simulation of the semiannual oscillation of the tropical middle atmosphere. *J. Atmos. Sci.,* **45,** 3212–3235.

Harries, J. E., S. Ruth, and J. M. Russell III, 1996a: On the distribution of mesospheric molecular hydrogen inferred from HALOE measurements of H_2O and CH_4. *Geophys. Res. Lett.,* **23,** 297–300.

——, and Coauthors, 1996b: Validation of measurements of water vapor from the Halogen Occultation Experiment. *J. Geophys. Res.,* **101,** 10 205–10 216.

Hitchman, M. H., M. McKay, and C. R. Trepte, 1994: A climatology of stratospheric aerosol. *J. Geophys. Res.,* **99,** 20 689–20 700.

Holton, J. R., and W.-K. Choi, 1988: Transport circulation deduced from SAMS trace species data. *J. Atmos. Sci.,* **45,** 1929–1939.

Jones, R. L., and J. A. Pyle, 1984: Observations of CH_4 and N_2O by the NIMBUS 7 SAMS: A comparison with in-situ data and two-dimensional numerical model calculations. *J. Geophys. Res.,* **89,** 5263–5279.

——, ——, J. E. Harries, A. M. Zavody, J. M. Russell III, and J. C. Gille, 1986: The water vapor budget of the stratosphere studied using LIMS and SAMS satellite data. *Quart. J. Roy. Meteor. Soc.,* **112,** 1127–1143.

Kelly, K. K., A. F. Tuck, L. E. Heidt, M. Loewenstein, J. F. Podolske, and S. E. Strahan, 1990: A comparison of ER-2 measurements of stratospheric water vapor between the 1987 Antarctic and 1989 Arctic airborn missions. *Geophys. Res. Lett.,* **17,** 465–468.

Kennaugh, R., S. Ruth, and L. J. Gray, 1997: Modeling quasi-biennial variability in the semi-annual double peak. *J. Geophys. Res.,* **102,** 16 169–16 188.

Kumer, J. B., J. L. Mergenthaler, and A. E. Roche, 1993: CLAES CH_4, N_2O and CCl_2F_2 (F_{12}) global data. *Geophys. Res. Lett.,* **20,** 1239–1242.

Lahoz, W. A., and Coauthors, 1996a: Vortex dynamics and the evolution of water vapor in the stratosphere of the Southern Hemisphere. *Quart. J. Roy. Meteor. Soc.,* **122,** 423–450.

——, and Coauthors, 1996b: Validation of UARS microwave limb sounder 183 GHz H_2O measurements. *J. Geophys. Res.,* **101,** 10 129–10 149.

Leovy, C. B., C.-R. Sun, M. H. Hitchman, E. E. Remsberg, J. M. Russell III, L. L. Gordley, J. C. Gille, and L. V. Lyjak, 1985: Transport of ozone in the middle stratosphere: Evidence for planetary wave breaking. *J. Atmos. Sci.,* **42,** 230–244.

LeTexier, H., S. Solomon, and R. R. Garcia, 1988: The role of molecular hydrogen and methane oxidation in the water vapor budget of the stratosphere. *Quart. J. Roy. Meteor. Soc.,* **114,** 281–295.

Luo, M., R. J. Cicerone, and J. M. Russell III, 1995: Analysis of Halogen Occultation Experiment HF versus CH_4 correlation plots: Chemistry and transport implications. *J. Geophys. Res.,* **100,** 13 927–13 437.

——, J. M. Russell III, and T. Y. W. Huang, 1997: HALOE observations of the quasi-biennial oscillation and the effects of Pinatubo aerosols in the tropical stratosphere. *J. Geophys. Res.,* **102,** 19 187–19 198.

Manney, G. L., R. W. Zurek, A.O'Neill, and R. Swinbank, 1994: On the motion of air through the stratospheric polar vortex. *J. Atmos. Sci.,* **51,** 2973–2994.

——, L. Froidevaux, J. W. Waters, and R. W. Zurek, 1995: Evolution of microwave limb sounder ozone and the polar vortex during winter. *J. Geophys. Res.*, **100,** 2953–2972.
McCormick, M. P., E. W. Chiou, L. R. McMaster, W. P. Chu, J. C. Larsen, D. Rind, and S. Oltmans, 1993: Annual variations of water vapor in the stratosphere and upper troposphere observed by the Stratospheric Aerosol and Gas Experiment II. *J. Geophys. Res.*, **98,** 4867–4874.
McIntyre, M. E., and T. N. Palmer, 1983: Breaking planetary waves in the stratosphere. *Nature*, **305,** 593–600.
——, and ——, 1984: The ''surf zone'' in the stratosphere. *J. Atmos. Terr. Phys.*, **46,** 825–849.
Mote, P. W., K. H. Rosenlof, J. R. Holton, R. S. Harwood, and J. W. Waters, 1995: Seasonal variations of water vapor in the tropical lower stratosphere. *Geophys. Res. Lett.*, **22,** 1093–1096.
——, and Coauthors, 1996: An atmospheric tape recorder: The imprint of tropical tropopause temperatures on stratospheric water vapor. *J. Geophys. Res.*, **101,** 3989–4006.
Newell, R. E., and S. Gould-Stewart, 1981: A stratospheric fountain? *J. Atmos. Sci.*, **38,** 2789–2796.
Norton, W. A., 1994: Breaking Rossby waves in a model stratosphere diagnosed by a vortex following coordinate system and a technique for advecting material contours. *J. Atmos. Sci.*, **51,** 654–673.
Olaguer, E. P., H. Yang, and K. K. Tung, 1992: A re-examination of the radiative balance of the stratosphere. *J. Atmos. Sci.*, **49,** 1242–1263.
O'Sullivan, D., 1997: Cross equatorially radiating stratospheric Rossby waves. *Geophys. Res. Lett.*, **24,** 1483–1486.
——, and P. Chen, 1996: Modeling the quasi-biennial oscillation's influence on isentropic tracer transport in the subtropics. *J. Geophys. Res.*, **101,** 6811–6821.
——, and T. J. Dunkerton, 1997: The influence of the quasi-biennial oscillation on global constituent distributions. *J. Geophys. Res.*, in press.
Park, J. H., and Coauthors, 1996: Validation of HALOE CH_4 measurements from UARS. *J. Geophys. Res.*, **101,** 10 183–10 204.
Pierce, R. B., W. Grose, J. R. Russell III, A. F. Tuck, R. Swinbank, and A. O'Neill, 1994: Spring dehydration in the Antarctic stratosphere vortex observed by HALOE. *J. Atmos. Sci.*, **51,** 2931–2941.
Plumb, R. A., and R. C. Bell, 1982: A model of the quasi-biennial oscillation on an equatorial beta-plane. *Quart. J. Roy. Meteor. Soc.*, **108,** 335–352.
Polvani, L. M., D. W. Waugh, and R. A. Plumb, 1995: On the subtropical edge of the stratospheric surf zone. *J. Atmos. Sci.*, **52,** 1288–1309.
Prather, M., and E. Remsberg, Eds., 1992: The atmospheric effects of stratospheric aircraft. NASA Ref. Publ. 1292, 268 pp.
Randel, W. J., and F. Wu, 1996: Isolation of the ozone QBO in SAGE II data by singular value decomposition. *J. Atmos. Sci.*, **53,** 2546–2559.
——, B. A. Boville, J. C. Gille, P. L. Bailey, S. T. Massie, J. B. Kumer, J. L. Mergenthaler, and A. E. Roche, 1994: Simulation of stratospheric N_2O in the NCAR CCM2: Comparison with CLAES data and global budget analysis. *J. Atmos. Sci.*, **51,** 2834–2845.
Remsberg, E. E., J. M. Russell III, L. L. Gordley, J. C. Gille, and P. L. Bailey, 1984: Implications of stratospheric water vapor distributions as determined from the Nimbus 7 LIMS Experiment. *J. Atmos. Sci.*, **41,** 2934–2945.
——, P. P. Bhatt, and J. M. Russell III, 1996: Estimates of the water vapor budget of the stratosphere from UARS HALOE data. *J. Geophys. Res.*, **101,** 6749–6766.
Roche, A. E., and Coauthors, 1996: Validation of CH_4 and N_2O measurements by the cryogenic limb array etalon spectrometer instrumention on the Upper Atmosphere Research Satellite. *J. Geophys. Res.*, **101,** 9679–9710.
Rosenfield, J., P. A. Newman, and M. R. Schoeberl, 1994: Computations of diabatic descent in the stratospheric polar vortex. *J. Geophys. Res.*, **99,** 16 677–16 689.
Rosenlof, K. H., 1995: Seasonal cycle of the residual mean meridional circulation in the stratosphere. *J. Geophys. Res.*, **100,** 5173–5191.
——, A. F. Tuck, K. K. Kelly, J. M. Russell III, and M. P. McCormick, 1997: Hemispheric asymmetries in water vapor and inferences about transport in the lower stratosphere. *J. Geophys. Res.*, **102,** 13 213–13 234.
Russell J. M., III, A. F. Tuck, L. L. Gordley, J. H. Park, S. R. Drayson, J. E. Harries, R. J. Cicerone, and P. J. Crutzen, 1993a: HALOE Antarctic observations in the spring of 1991. *Geophys. Res. Lett.*, **20,** 719–722.
——, and Coauthors, 1993b: The Halogen Occultation Experiment. *J. Geophys. Res.*, **98,** 10 777–10 797.
Ruth, S., R. Kennaugh, and L. J. Gray, 1997: Seasonal, semiannual and interannual variability seen in measurements of methane made by the UARS Halogen Occultation Experiment. *J. Geophys. Res.*, **102,** 16 189–16 200.
Sassi, F., R. R. Garcia, and B. A. Boville, 1993: The stratopause semiannual oscillation in the NCAR community climate model. *J. Atmos. Sci.*, **50,** 3608–3624.
Schoeberl, M. R., and Coauthors, 1989: Reconstruction of the constituent distribution and trends in the Antarctic polar vortex from ER-2 flight observations. *J. Geophys. Res.*, **94,** 16 815–16 846.
——, L. R. Lait, P. A. Newman, and J. E. Rosenfield, 1992: The structure of the polar vortex. *J. Geophys. Res.*, **97,** 7859–7882.
——, M. Luo, and J. E. Rosenfield, 1995: An analysis of the Antarctic Halogen Occultation Experiment trace gas observations. *J. Geophys. Res.*, **100,** 5159–5172.
——, A. E. Roche, J. M. Russell III, D. Ortland, P. B. Hays, and J. W. Waters, 1997: An estimation of the dynamical isolation of the tropical lower stratosphere using UARS wind and trace gas observations of the quasi-biennial oscillation. *Geophys. Res. Lett.*, **24,** 53–56.
Solomon, S., J. T. Kiehl, R. R. Garcia, and W. Grose, 1986: Tracer transport by the diabatic circulation deduced from satellite observations. *J. Atmos. Sci.*, **43,** 1603–1617.
Stanford, J. L., J. R. Ziemke, and S. Y. Gao, 1993: Stratospheric circulation features deduced from SAMS constituent data. *J. Atmos. Sci.*, **50,** 226–246.
Strahan, S. E., J. E. Nielsen, and M. C. Cerniglia, 1996: Long-lived tracer transport in the Antarctic stratosphere. *J. Geophys. Res.*, **101,** 26 615–26 629.
Sutton, R., 1994: Lagrangian flow in the middle atmosphere. *Quart. J. Roy. Meteor. Soc.*, **120,** 1299–1321.
Swinbank, R., and A. O'Neill, 1994: A stratosphere–troposphere data assimilation system. *Mon. Wea. Rev.*, **122,** 686–702.
Trepte, C. R., and M. H. Hitchman, 1992: Tropical stratospheric circulation deduced from satellite aerosol data. *Nature*, **355,** 626–628.
——, R. E. Veiga, and M. P. McCormick, 1993: The poleward dispersal of the Mt. Pinatubo volcanic aerosol. *J. Geophys. Res.*, **98,** 18 562–18 573.
Tuck, A. F., J. M. Russell III, and J. E. Harries, 1993: Stratospheric dryness: Antiphased dessication over Micronesia and Antarctica. *Geophys. Res. Lett.*, **20,** 1227–1230.
Volk, C. M., and Coauthors, 1996: Quantifying transport between the tropical and midlatitude lower stratosphere. *Science*, **272,** 1763–1768.
Wallace, J. M., R. L. Panetta, and J. Estberg, 1993: Representation of the equatorial quasi-biennial oscillation in EOF phase space. *J. Atmos. Sci.*, **50,** 1751–1762.
Waugh, D. W., 1996: Seasonal variation of isentropic transport out of the tropical stratosphere. *J. Geophys. Res.*, **101,** 4007–4023.
Zawodny, J. M., and M. P. McCormick, 1991: Stratospheric aerosol and gas experiment II measurements of the quasi-biennial oscillation in ozone and nitrogen dioxide. *J. Geophys. Res.*, **96,** 9371–9377.